Report No. KS-03-6
FINAL REPORT

FIELD INSTRUMENTATION AND ANALYSIS OF THE ARKANSAS RIVER BRIDGE
Bridge No. 96-78-19.11(064)

Kaise Haris
Guillermo Ramirez, Ph.D., P.E.
W. M. Kim Roddis, Ph.D., P.E.
University of Kansas

SEPTEMBER 2004

KANSAS DEPARTMENT OF TRANSPORTATION

Division of Operations
Bureau of Materials and Research

1 Report No. KS-03-6	**2 Government Accession No.**	**3 Recipient Catalog No.**
4 Title and Subtitle **FIELD INSTRUMENTATION AND ANALYSIS OF THE ARKANSAS RIVER BRIDGE** ***BridgeNo. 96-78-19.11(064)***		**5 Report Date** September 2004 **6 Performing Organization Code**
7 Author(s) Kaise Haris, Guillermo Ramirez, Ph.D., P.E., and W. M. Kim Roddis, Ph.D., P.E.		**8 Performing Organization Report No.**
9 Performing Organization Name and Address University of Kansas 1530 West 15th Street Lawrence, KS 66045		**10 Work Unit No. (TRAIS)** **11 Contract or Grant No.**
12 Sponsoring Agency Name and Address Kansas Department of Transportation Bureau of Materials and Research 700 SW Harrison Street Topeka, Kansas 66603		**13 Type of Report and Period Covered** Final Report February 1998 – September 2003 **14 Sponsoring Agency Code** 96-78 K-6879-01

15 Supplementary Notes
For more information write to address in block 9.

16 Abstract

A field instrumentation analysis has been performed on the Arkansas River Bridge, [KDOT Bridge No. 96-78-19.11(064)]. The testing was performed before and after retrofit on the exterior girder to floor-beam connections. Before retrofit, the measured stresses match the computational ANSYS results at the stiffener plate. Fatigue life calculations for the retrofitted detail indicated a time range to crack initiation of 25 to 65 years. Calculated fatigue lives are inherently uncertain due to variability in measured stresses, traffic forecast, and construction details. Because the inspected and repaired cracks had not propagated into the web of the main beams before the retrofit it is reasonable to conclude that when a fatigue crack reinitiates stable crack growth will remain in the stiffener. This retrofit of softening the connections was successful, both in repairing existing cracks which were growing in the heat-affected zone of the welds and in softening the connection to mitigate the out-of-plane distortion driven strain-induced fatigue.

17 Key Words Bridges, Cracking, Fatigue, Girders and Repair	**18 Distribution Statement** No restrictions. This document is available to the public through the National Technical Information Service, Springfield, Virginia 22161

19 Security Classification (of this report) Unclassified	**20 Security Classification (of this page)** Unclassified	**21 No. of pages** 61	**22 Price**

Form DOT F 1700.7 (8-72)

FIELD INSTRUMENTATION AND ANALYSIS

OF THE ARKANSAS RIVER BRIDGE

Bridge No. 96-78-19.11(064)

Final Report

Prepared by

Kaise Haris

Guillermo Ramirez, Ph.D., P.E.

W. M. Kim Roddis, Ph.D., P.E.

A Report on Research Sponsored By

THE KANSAS DEPARTMENT OF TRANSPORTATION
TOPEKA, KANSAS

UNIVERSITY OF KANSAS
LAWRENCE, KANSAS
KUCR Project Number KAN27580

September 2004

NOTICE

DISCLAIMER

ABSTRACT

A field instrumentation analysis has been performed on the Arkansas River Bridge, [KDOT Bridge No. 96-78-19.11(064)]. The testing was performed before and after retrofit on the exterior girder to floor-beam connections. Before retrofit, the measured stresses match the computational ANSYS results at the stiffener plate. Fatigue life calculations for the retrofitted detail indicated a time range to crack initiation of 25 to 65 years. Calculated fatigue lives are inherently uncertain due to variability in measured stresses, traffic forecast, and construction details. Because the inspected and repaired cracks had not propagated into the web of the main beams before the retrofit it is reasonable to conclude that when a fatigue crack reinitiates stable crack growth will remain in the stiffener. This retrofit of softening the connections was successful, both in repairing existing cracks which were growing in the heat-affected zone of the welds and in softening the connection to mitigate the out-of-plane distortion driven strain-induced fatigue.

TABLE OF CONTENTS

LIST OF FIGURES

LIST OF TABLES

SECTION 1 INTRODUCTION

The four-lane Arkansas River Bridge [KDOT Bridge No. 96-78-19.11(064)], designed in 1949 and constructed in 1955, has experienced fatigue cracking and various other problems throughout its lifetime. This report consists of a field instrumentation analysis comparing the predicted internal stresses based on computational analysis to actual measured conditions. The computational analysis, performed by Dr. Roddis and Dr. Zhao, is entitled “An Investigation and Retrofit Recommendation for Cracking of the Arkansas River Bridge” (Zhao and Roddis, 2001). The final report performed by Dr. Roddis and Dr. Zhao, is titled “Fatigue-Prone Steel Bridge Details: Investigations and Recommended Repairs” (Zhao and Roddis, 2003). The present report is a follow-up of the above referenced research, with the primary purpose of measuring the stress range before and after retrofit.

Extensive work applying fatigue and fracture mechanics, as well as an ANSYS coarse model to submodel computational analysis, was performed to predict internal stresses at critical locations where the exterior floor-beam connections have experienced fatigue cracks at the stiffener plates. In addition to predicting internal stresses, Dr. Roddis and Dr. Zhao have provided a retrofit concept to extend the fatigue life of the exterior floor-beam connections. The retrofit repairs existing cracks and “softens” the connection, making the connection less rigid. The retrofit eliminates the AASHTO category-C detail and replaces it with a category-A detail (base metal of stiffener). The stiffener plates at the exterior floor-beam connections were partially cut short with a 3” radius providing a smooth transition for forces due to floor-beam end rotations, as shown in Appendix D, Sheet 7, Detail A. For the field instrumentation, 24 gages were installed before and after retrofit. Trucks of known weights were used to load the bridge.

The stresses were measured at specified locations, and a comparison was made between computed and measured stresses.

SECTION 2 FIELD INSTRUMENTATION

Field-testing was performed before and after retrofit of the bridge to measure the actual stress conditions under different loading conditions. A description of all the instruments and accessories used, the procedure followed for installation, preparations for field instrumentation, and the procedure used for testing is presented in the following sections.

2.1 Description of the Instruments Used During Testing

This section describes the instrumentation used for the field-testing. Instrumentation includes: strain gages, the data acquisitions system, the Waveview software, and other necessary accessories (Vishay Measurements Group, Inc., 2000) (IOtech, Inc., 1997).

2.1.1 Gages Used for Field Instrumentation Prior-to-Retrofit

Twenty-four strain gages were to be installed before and after retrofit of the Arkansas River Bridge. Due to a defect in one of the channels in the data acquisition system, only 23 of the 24 channels were used. The strain gages were obtained from Micro Measurements Group, Inc. For the prior-to-retrofit testing, two types of gages were installed. Only one type will be described because this type of gage is the only gage used to provide stress ranges within the context of this report.

Twenty-one single-element strain gages, with the Micro Measurements specification as CEA-06-250UW-350, were used. This gage is called a single-element gage because strain is measured in one direction. This gage has a resistance of 350 ± 3% ohms and an exposed soldering tab area of 0.10”x0.07”. The gage factor is 2.10 ± 5%, which is a required input factor to the data acquisition system. This gage factor is representative of the sensitivity of the output from the strain gage. This gage was specifically chosen for two reasons. First, the designation CE specifies that the gage be composed of a cast-polyimide backing with soldering tabs that are large, rugged, and copper-coated. Easy soldering capabilities were important because the soldering was performed under the bridge on the Mark II snooper platform with traffic flowing so that substantial vibrations were present. Second, this gage has a self-temperature compensation, indicated by the A designation, suitable for the possible changes in temperature during testing.

2.1.2 Gages Used in Instrumentation Following Retrofit

Following retrofit, 23 strain gages, composed of three different types, were installed. Only two of the three types of gages will be discussed because of the stress ranges of interest in this report. Nine strain gages were used with the Micro Measurements, Inc. designation of CEA-06-250UW-350, the single-element gage described previously. Four large three-element delta rosettes, which have the gages oriented 45˚ from each other, were installed. These rosettes have a resistance of 350 ± 4% ohms and an exposed soldering tab area of 0.13”x0.08”. The nominal gage factor is 2.10 ± 1%.

2.1.3 Data Acquisition System Description

The data acquisition system is composed of a laptop computer, one Wavebook, and three strain gage modules. The laptop is a Dell Latitude CP*i*. The Wavebook, specified as a WB516 and purchased from Iotech, Inc., is a high-speed Waveform Data Acquisition and Analysis Module. The three strain gage modules, specified as

Figure 2.1.3.1: Instrumentation Setup

WBK16/SSH modules, each have eight channels to provide the 24 channels required for testing. Each channel has a cable that runs to a terminal strip. The wires run from the strain gage to a terminal strip with a quarter bridge configuration. Figure 2.1.3.1 shows the entire data acquisition system fully installed in the field.

2.1.4 Waveview Software Description

IOtech's Waveview 7.12.5 is the software used to acquire the data from the strain gages during testing. This software enables easy calibration and channel configuration of the strain gages. From this software, a data file is produced during testing that can be imported into Excel for analysis purposes.

2.1.5 Description of Other Required Accessories

In addition to the strain gages and the data acquisition software and hardware, other accessories were required for the instrumentational analysis of the Arkansas River Bridge. Some of these accessories included the wires that led from the strain gages to the terminal strips, which are specified by Micro Measurements as 326DFV. The other necessary accessories to properly install the gages onto the bridge will not be discussed because they are assumed to be standard. At the time of installation, the other equipment required included the Mark II snooper and an operator, as shown in Figure 2.1.5.1. A portable generator at the site was also necessary, in addition to hard hats and safety vests for the installers. For loading, two HS15 dump trucks were provided, as shown in Figure 2.1.5.2, with known weights and wheel dimensions. Lamps were required to light the working area and to heat the steel prior to installation.

Figure 2.1.5.1: Mark II Snooper

Picture 2.1.5.2: HS15 Trucks

2.2 Preparation for Installation

Several preparatory tasks were done to limit the amount of field installation work. The Waveview program's calibration file was created for the configuration that would be used. The wires that ran from the strain gage were cut to the necessary lengths required to run from the connection being tested to the terminal strips at the top of the bridge deck. The wires were stripped for about two inches for quick soldering to the gages. These exposed wires were covered in tape prior to installation to prevent any contamination. At the other end of the wires, the spade-tongue terminals were soldered for quick attachment to the terminal strips. The cables that ran from the modules to the terminal strips had their spade-tongue terminals properly soldered. The strain gages were taken from their package and applied to a plastic pad with tape for quick accessibility to the gages in the testing site. All channels, cables, and wires were tested prior to field installation.

2.3 On Site Installation Procedure

The first step in the procedure on site was to remove the drainage tubes that interfered with accessibility to the connections being tested. The driving lane was blocked off so that the Mark II snooper could be placed above the connections to be tested. The installers were required to wear hard hats, safety vests, and safety harnesses attached to the handrail of the snooper platform. Before installation, the steel at the locations of the gages was sandblasted, with a smoothness specification of SSPC-SP6. After proper installation of the strain gages, the exact location of the gages was documented. Marine goop was applied to the strain gages after the wires were soldered to the gages. This protected the gages from the environment. Figure 2.3.1 shows gages installed at one connection prior to the application of the marine goop. This field installation procedure required 2.5 days before retrofit and 1.5 days after retrofit.

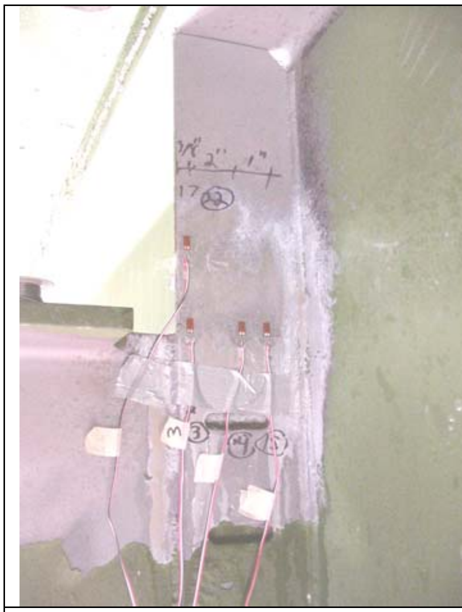

Figure 2.3.1: Strain Gages Installed

2.4 Testing Procedure

For the testing procedure, two HS15 trucks were supplied by KDOT before and after retrofit. The bridge was blocked off from traffic during the testing and all construction work on the bridge was temporarily halted. Before retrofit, 21 loading conditions were applied. After retrofit, seven loading conditions were applied. Each loading condition was executed twice. The trucks drove from south to north and data was recorded at a rate of 200 data points per second to ensure that the peak stresses were captured. For each loading condition, the data recording was initiated just as the front tire of the HS15 truck was running over the expansion joint at pier #5. For prior-to-retrofit testing, a pre-trigger was set for 5 seconds before the activation of data recording. In addition, prior-to-retrofit, the data recording was terminated when the front wheels of the truck ran over the expansion joint at pier #12. Due to the realization that some vibrations were still occurring after the trucks ran over the expansion joint at pier #12 on some gages, a correction was made following retrofit. These complete stress curves were captured after retrofit by terminating the data recording 184' after the expansion joint at pier #12. The testing required four hours prior-to-retrofit and two hours after retrofit.

SECTION 3 GAGE AND CONNECTION DESIGNATIONS

For the instrumentation analysis, 23 gages were analyzed before and after retrofit. The systematic designation presented below is used for gages and connections for clarity in the analysis and comparisons presentation. Repair plans are presented in Appendix D.

Designation for gages:

$$G-(Number)_1-(Number)_2-(Letter)_1-(Letter)_2-(Letter)_3$$

Designation for connections:

$$FB(Number)_1-(Number)_2-(Letter)_1-(Letter)_2$$

Where:

G = Gage Designation

FB = Floor-beam Connection Designation

$(Number)_1$ = Span number as indicated on bridge repair plans where connection is located, designated as 10 or 11.

$(Number)_2$ = Floor-beam number as indicated on bridge repair plans where connection is located, designated as 1 or 2.

$(Letter)_1$ = Girder where connection is located, designated as D, as indicated on bridge repair plans.

$(Letter)_2$ = Direction of the face at the connection where the gage is located, designated as N or S.

$(Letter)_3$ = Gage location designation as explained below, designated as A through P.

The connections tested are:

FB10-2-D-N

FB10-2-D-S

FB11-1-D-N

FB11-1-D-S

3.1 Gage Designations Prior-to-Retrofit

Figure 3.1.1 shows gage location designated A, B, C, and D. Gage locations A, B, and C are located on the stiffener plate, just above the floor-beam top flange. Gage D is installed about 3” above the top flange of the floor-beam. The gage designations A, B, C, and D apply to either side of the stiffener plate.

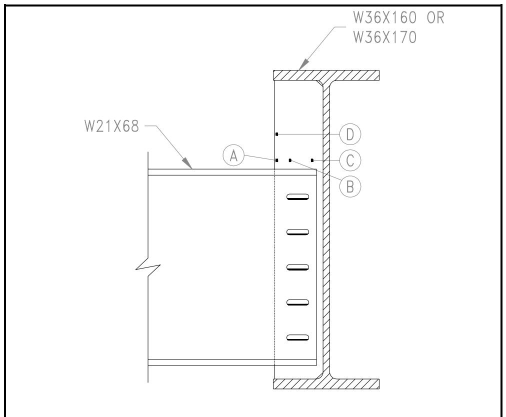

Figure 3.1.1: Exterior Girder D Connection Gage Designations Prior-to-Retrofit

3.2 Gage Designations After Retrofit

Gages A, B, C, and D at the girder D connections were replaced with rosettes because of the configuration of the retrofit at the connections. Each rosette was composed of three strain gages spaced 45˚ apart. These gages locations are designated K, L, M, N, O, and P, as depicted in Figure 3.2.1.

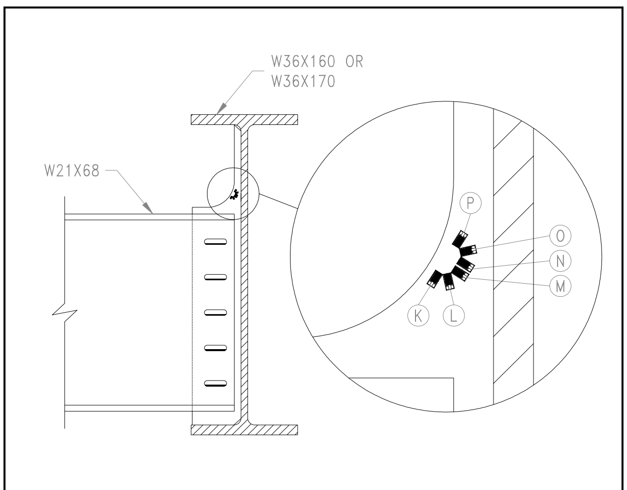

Figure 3.2.1: Exterior Girder D Gage Designations Following Retrofit

SECTION 4 COMPARISON OF COMPUTED VERSUS MEASURED RESULTS BEFORE RETROFIT

The results from computational analysis of the connection before retrofit are summarized and compared to the results from field measurements. For this comparison of results prior-to-retrofit, the computational model results performed by Dr. Zhao and Dr. Roddis are first presented. The installed gage locations and loading conditions are defined. The data conditioning using a moving average technique is explained. Then, instrumentation analysis results are presented.

4.1 ANSYS Model Results

For computational results using the ANSYS program, a submodel was created after the coarse model was developed. The stress contours are presented in Figure 4.1.1 for the prior-to-retrofit analysis, assuming no cracks exist in the stiffener plate. This figure shows the stress distribution contours at the connection to be retrofitted. The loading for this model is an HS15 truck, located in the driving lane, with an increase of 10% for dynamic effects. Further details about the models are documented in the computational analysis reports (Zhao and Roddis, 2001, 2003).

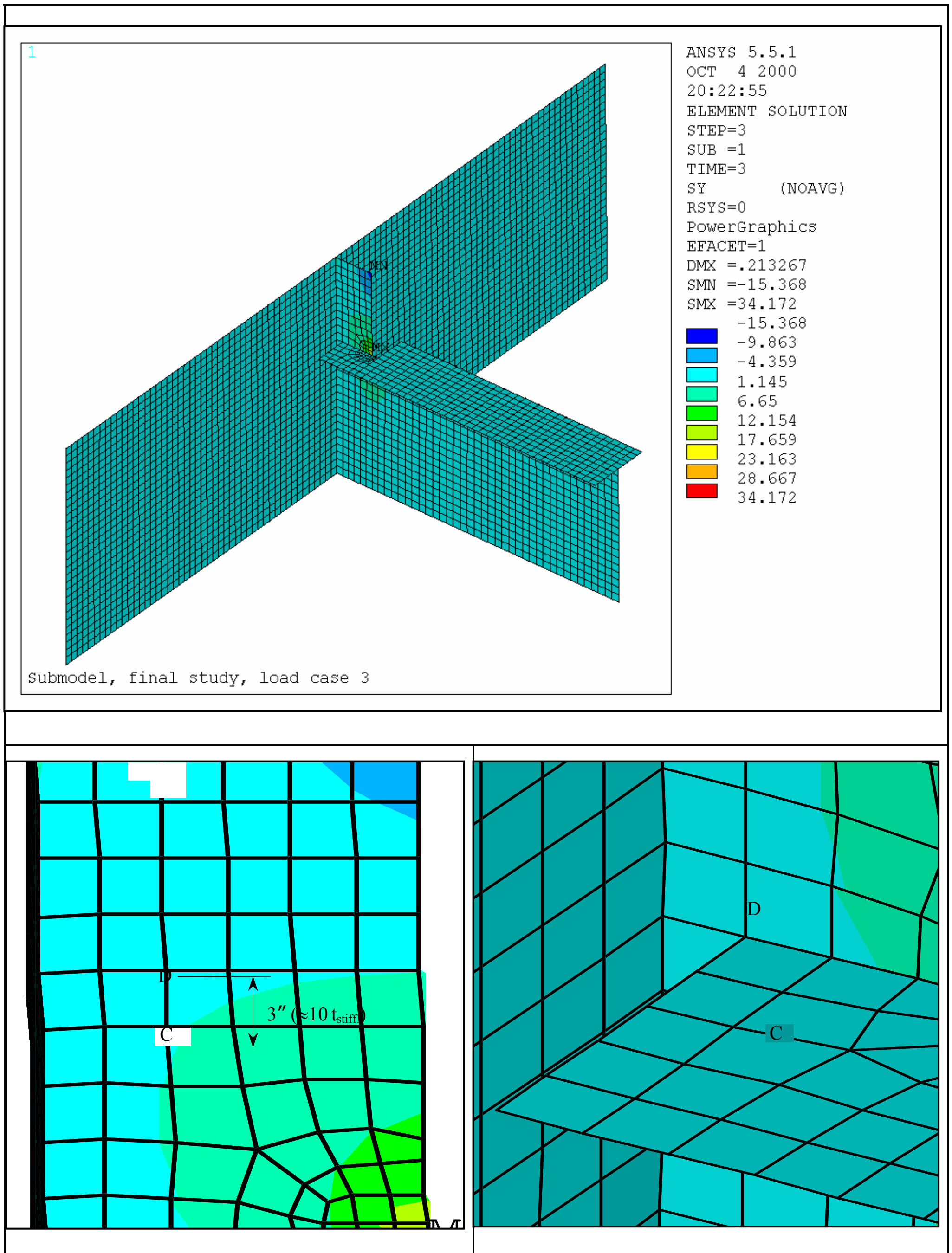

Figure 4.1.1: ANSYS Submodel Prior-to-Retrofit
(Zhao and Roddis, 2001, 2003)

As observed in these figures, point C is the stress concentration point where the stresses reach 34 ksi. Point D, 3" above the stress concentration point, has stresses from 1.1 ksi to 6.6 ksi. Point D, located approximately 10 times the plate thickness away from the stress concentration point, is used to determine stress ranges for fatigue life calculations using the AASHTO fatigue category approach. The AASHTO fatigue category detail characterization takes into account stress concentrations, residual stresses, initial flaws, and material variability in the tests (Xanthakos, 1994) (AASHTO Fatigue Guide, 1990).

4.2 Strain Gage Locations Prior-to-Retrofit

The exact locations of the strain gages are provided below prior-to-retrofit for the gages of interest in this report. The dimensions are shown in Figures 4.2.1-4. As shown in Figure 4.2.2, gage C is not presented because the results showed that this gage was defective. The exact dimensions of the gages are not equal, due to the difference in surface smoothness of the steel. Strain gage installation requires the surface of the steel to be as smooth as possible in order to obtain a good bond.

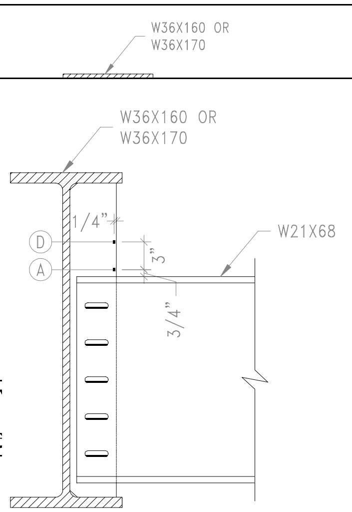

F s at
Conne -Retrofit

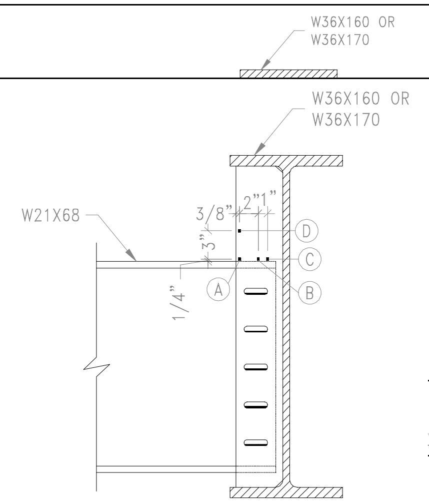

Cc rofit

Figure 4.2.3: Gage Locations at Connection FB11-1-D-N Prior-to-Retrofit

Figure 4.2.4: Gage Locations at Connection FB11-1-D-S Prior-to-Retrofit

4.3 Loading Conditions Prior-to-Retrofit

The loading conditions in the scope of this report used a truck of known weight in the driving lane traveling at a speed of about 10 or 30 mph. Loading condition 2 is a repeat of loading condition 1. Loading condition 4 is a repeat of loading condition 3. Table 4.3.1 provides the actual trucks' weights for each loading condition and a calculated velocity based on the duration of data recording.

Table 4.3.1
Loading Conditions Prior-to-Retrofit with Truck Traveling in Driving Lane

Loading Condition	Truck Weight (kips)	Desired Velocity (mph)	Duration of Recording (sec.)	Calculated Velocity (mph)
1	59.64	10	25	11.45
2	59.32	10	25	11.45
3	59.64	30	11	26.03
4	59.32	30	11	26.03

4.4 Moving Average Technique

All the data recorded had an amount of scatter in voltages that is not representative of the actual strains. A moving average technique was used to condition the raw data, removing the scatter due to noise to prepare the data for analysis. This technique was applied using a spreadsheet built-in function to average the specified preceding number of data points, as expressed by the following formula:

$$A_{t+1} = \frac{1}{n}\sum_{i-n}^{n} s_{t-i+1} \qquad \text{(Equation 4.4.1)}$$

Where:

A_{t+1} = Moving average data point

s_{t-i+1} = Recorded data point

n = Number of preceding data points specified

This procedure can be used to eliminate scatter or noise as shown in Figure 4.4.1.

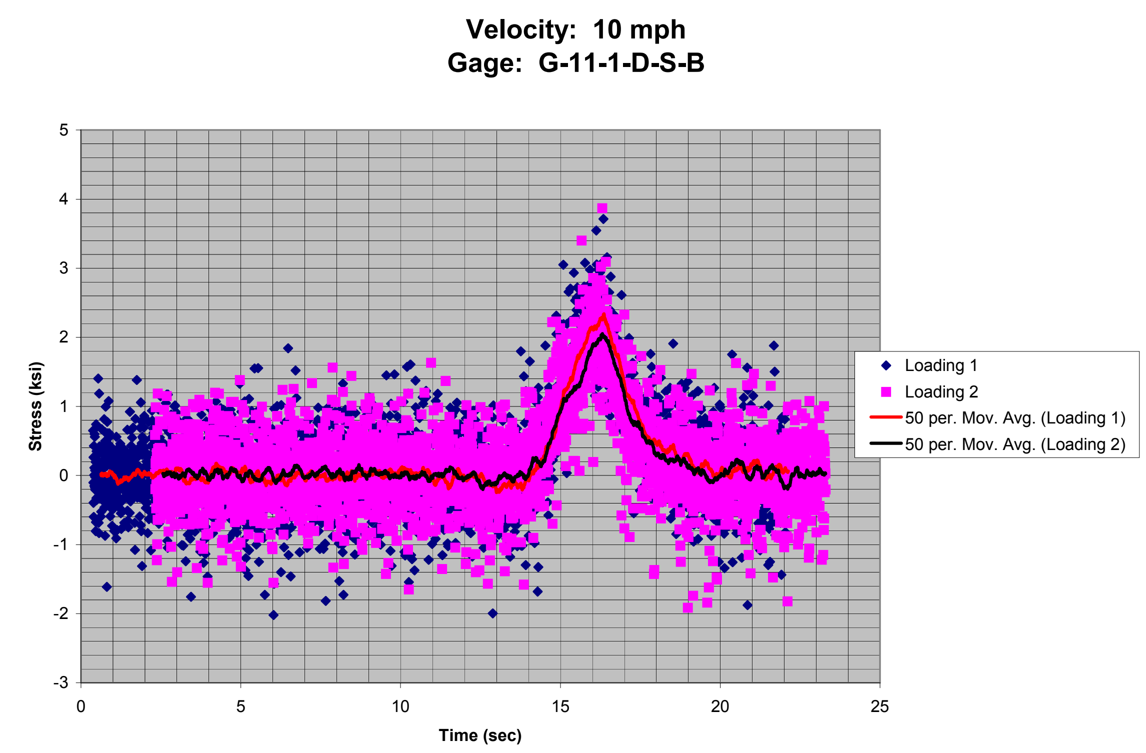

Figure 4.4.1: Moving Average Plot

This graph emphasizes the importance of utilizing the moving average to obtain the $\Delta \sigma$ stresses. The n value used in all calculations of this report was 50. Each point in the moving average curve is the average of the previous 50 data points at a frequency of 200 data points per second.

4.5 Strain Gage Results Prior-to-Retrofit

The $\Delta \sigma$ stress ranges computed from strain gages A, B, C, and D measurements were plotted versus horizontal distance from the edges of the stiffener and vertical distance from top of the floor-beam. Figure 4.5.1 show that the measured stresses match well with the computed ANSYS stresses. Near the stress concentration, the measured stresses are greater than the computed stresses. The gages closest to the edge of the stiffener, G-11-1-D-S-A, G-11-1-D-N-A, G-10-2-D-S-A, and G-10-2-D-N-A, shows this most clearly in Figure 4.5.1 since these gages are closest to the stress concentration.

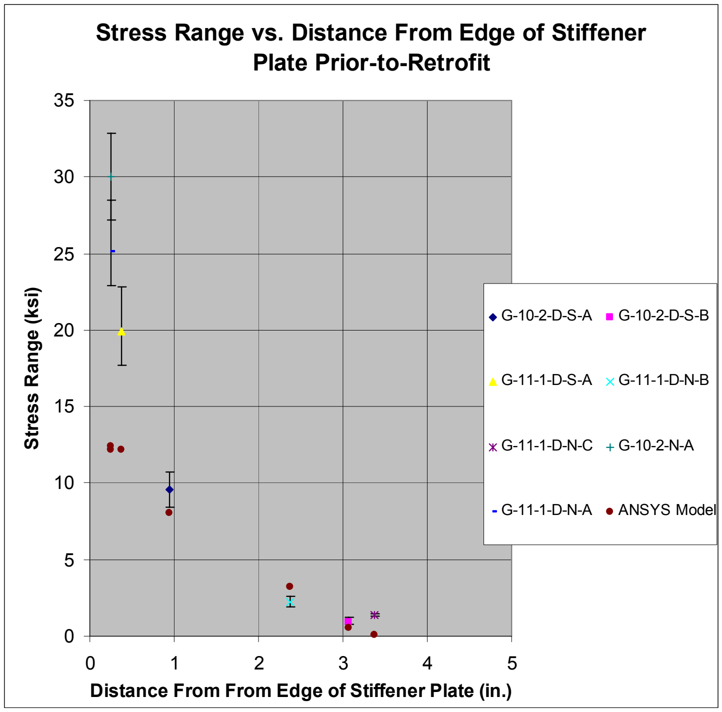

Figure 4.5.1

At 3” away from the stiffener plate edge, both connections have approximately the same stress. This stresses match at the distance of 3” (10 times the plate thickness) used for determining the stress range outside of the concentration zone (Zhao and Roddis, 2001, 2003, Section 5.3.2).

Gages A and D are plotted versus the distance from the top of the top flange of the floor-beam. In Figure 4.5.2 the stresses from the ANSYS computational model are all significantly lower than the gage stresses, with the exception of G-10-2-D-S-A. That is to say, the gages that are within 3/8” from the edge of stiffener or weld indicate higher stresses than the ANSYS model, while the one gage close to 1” from the edge agrees closely with the ANSYS model.

Since both the gages and the ANSYS model assume linear elastic behavior, while the actual material can yield in the region of a high stress concentration, this discrepancy is understandable and acceptable in light of the use of the far-field stresses in predicting fatigue life. Indeed, the G-10-2-D-S-A reading indicates that at 1" away from the edge of the stiffener plate edge, there are no effects due to the stress concentrations. The G-10-2-D-S-A stress closely matches the ANSYS model stress of 5.6 ksi for the unretrofitted fatigue life calculations (Zhao and Roddis, 2001, 2003, Section 5.3.2).

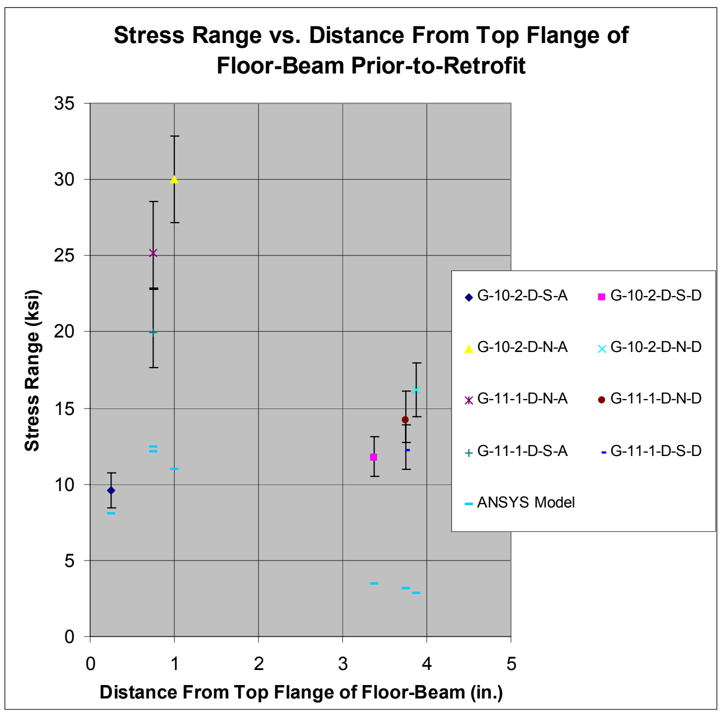

Figure 4.5.2

SECTION 5 COMPARISON OF COMPUTED VERSUS MEASURED RESULTS AFTER RETROFIT

The computational model results and actual measured principal stresses are compared following retrofit. The strain gage locations and loadings conditions are presented. The equations used for the principal stress calculations are discussed. Then, the resulting principal stresses are compared.

5.1 Strain Gage Locations Following Retrofit

The locations of the strain gages are provided in Figure 5.1.1-2 following retrofit for the gages of interest in this report. The dimensions of the rosettes are not equal at both connections due to the difference in geometry of the partially cut short stiffener plates.

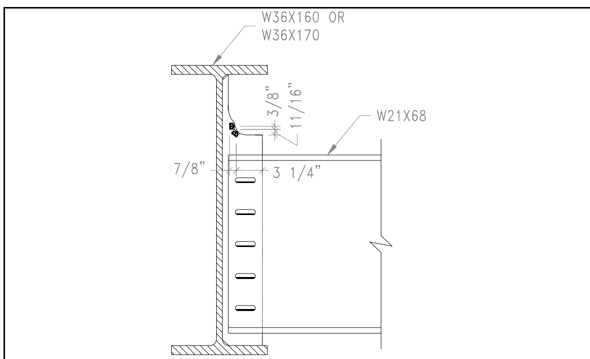

Figure 5.1.1: Gage Locations at Connection FB10-2-D-N Following Retrofit

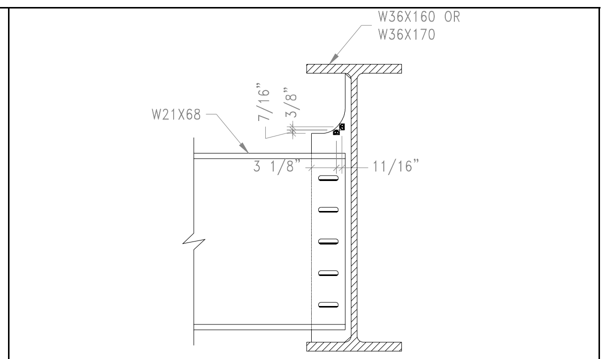

Figure 5.1.2: Gage Locations at Connection FB11-1-D-S Following Retrofit

5.2 Loading Conditions Following Retrofit

Table 5.2.1 provides the actual trucks' weights for each loading condition and a calculated velocity based on the duration of data recording.

Table 5.2.1 Loading Conditions Following Retrofit with Truck Traveling in Driving Lane				
Loading Condition	Truck Weight (kips)	Desired Velocity (mph)	Duration of Recording (sec.)	Calculated Velocity (mph)
1	57.82	10	35	11.76
2	56.74	10	35	11.76
3	57.82	30	15	27.44
4	56.74	30	15	27.44

5.3 Principal Stress Calculations

The principal stresses and angles are obtained from the readings of the rosette gages. Figure 5.3.1 depicts a typical rosette.

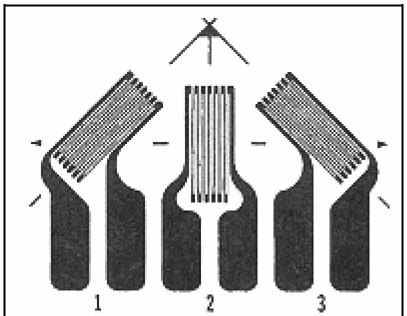

Figure 5.3.1: Rosette

Figure 5.3.2 shows the terminology used to define gages that are part of the rosette, and their orientations.

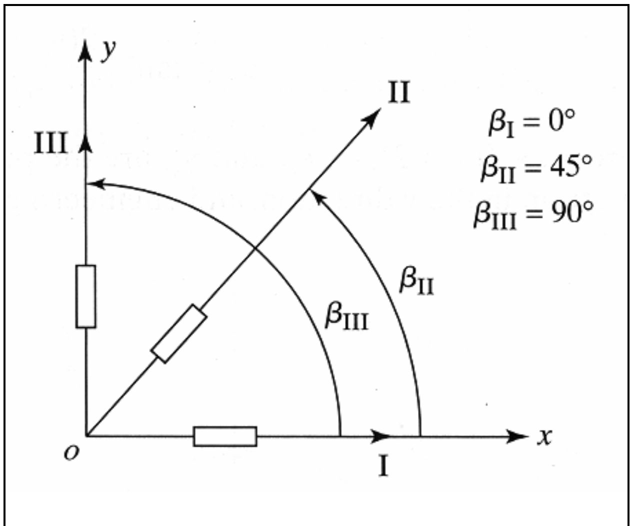

Figure 5.3.2: Rosette Designations

The following equations are valid for $\varepsilon_1 > \varepsilon_2 > \varepsilon_3$. The 1st principal stress is calculated as:

$$\sigma_1 = E\left\{\frac{\varepsilon_{\mathrm{I}} + \varepsilon_{\mathrm{II}}}{2(1-\mu)} + \frac{1}{2(1+\mu)}\left[(\varepsilon_{\mathrm{I}} + \varepsilon_{\mathrm{III}})^2 + (2\varepsilon_{\mathrm{II}} - \varepsilon_{\mathrm{I}} - \varepsilon_{\mathrm{III}})^2\right]^{1/2}\right\} \qquad \text{(Equation 5.3.1)}$$

The 2nd principal stress is defined as:

$$\sigma_2 = E\left\{\frac{\varepsilon_{\mathrm{I}} + \varepsilon_{\mathrm{II}}}{2(1-\mu)} - \frac{1}{2(1+\mu)}\left[(\varepsilon_{\mathrm{I}} + \varepsilon_{\mathrm{III}})^2 + (2\varepsilon_{\mathrm{II}} - \varepsilon_{\mathrm{I}} - \varepsilon_{\mathrm{III}})^2\right]^{1/2}\right\} \qquad \text{(Equation 5.3.2)}$$

The 1st and 2nd principal angles are calculated as:

$$\alpha_1 = \tan^{-1}\frac{2\varepsilon_{\mathrm{II}} - \varepsilon_{\mathrm{I}} - \varepsilon_{\mathrm{III}}}{2(\varepsilon_{\mathrm{I}} - \varepsilon_{\mathrm{III}})} \qquad \text{(Equation 5.3.3)}$$

$$\alpha_2 = \alpha_1 + 90° \qquad \text{(Equation 5.3.4)}$$

Where:

σ_1 = 1st principal stress

σ_2 = 2nd principal stress

α_1 = 1st principal angle

α_2 = 2nd principal angle

$\varepsilon_1, \varepsilon_2, \varepsilon_3 =$ Measured strains

$E =$ Modulus of elasticity

(Daily and Riley, 1991)

The calculation of principal stresses using Equations 5.3.1-4 applies to one state of stress and at one point in the plate and one instance of time. Since the maximum and minimum values in the strain gages do not necessarily occur at the same time for each gage, or in exactly the same direction, the following approach was used for the computation of the principal stresses and angles. The principal stresses and angles were first found for each time increment of the conditioned data (see Section 4.4 for description of data conditioning). Then, the maximum 1st principal stress and its corresponding angle and 2nd principal stress and angle were found. This approach was taken due to the small magnitudes of the minimum principal stresses for loading condition 1 and 2. For all four rosettes these minimum 1st compressive principal stresses are about 0.70 ksi. These small compressive stresses in these locations are due to shear, not direct compression. It is conservative to neglect small compressive stresses for determining stress ranges since the compressive portion of the cycle would actually retard crack growth, as accounted for in the stress ratio R used in fatigue calculations. Since the minimum strains in each gage were not used in the calculations, the stress ranges are assumed to be the full tensile range. Appendix A provides stress recordings versus time plot of each gage of the rosettes at both connections for loading conditions 1 and 2.

5.4 After-Retrofit Comparisons

Following retrofit, the main comparison to be made w computational model and the principal stresses measured. For the computational analysis, a maximum principal stress was given as a $\Delta\sigma$ of 23.79 ksi, which is the maximum 1st principal stress range. Therefore, this number will be used for comparison and the location of interest designated as point P4 in Figure 5.4.1. Note the analytically modeled retrofit differs from the constructed retrofit. The remaining stiffener height on the repair plans is 2", not ¾", due to construction feasibility. The measured heights at the two connections tested are 2½". The principal stresses for loadings 1 to 4 are provided in Tables 5.4.1-2.

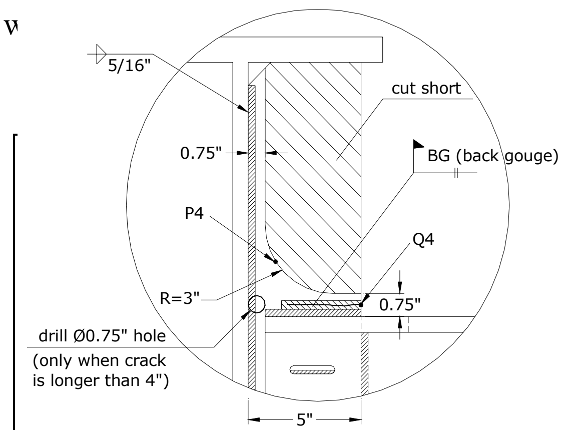

Figure 5.4.1: Retrofit of Floor-Beam to Exterior Girder Connections (Zhao and Roddis, 2001, 2003)

As observed in the following tables, loadings 1 and 2 induce larger stresses than loadings 3 and 4, but this difference in magnitudes is so small that no conclusion can be made about trucks traveling at higher velocities inducing smaller stresses.

A graphical presentation of the stresses on the curved portion of the cut short stiffener plate emphasizes the validity of the principal stress calculations. Presented in Figures 5.4.2-5 are the principal stresses and directions due to loading cases 1 and 2 on both connections.

Table 5.4.1

Gage	Loading 1 1st Principal Stress (ksi)	Loading 1 2nd Principal Stress (ksi)	Loading 1 1st Principal Angle (rad)	Loading 2 1st Principal Stress (ksi)	Loading 2 2nd Principal Stress (ksi)	Loading 2 1st Principal Angle (rad)
G-10-2-D-N-K G-10-2-D-N-L G-10-2-D-N-M	27.29	4.06	-17.31	26.90	3.98	-17.41
G-10-2-D-N-N G-10-2-D-N-O G-10-2-D-N-P	28.84	2.94	-30.93	28.60	2.92	-30.86
G-11-1-D-S-K G-11-1-D-S-L G-11-1-D-S-M	25.73	5.41	-2.15	25.35	4.70	-0.51
G-11-1-D-S-N G-11-1-D-S-O G-11-1-D-S-P	40.46	7.99	-24.16	34.54	6.38	-22.20

Table 5.4.2

Gage	Loading 3 1st Principal Stress (ksi)	Loading 3 2nd Principal Stress (ksi)	Loading 3 1st Principal Angle (rad)	Loading 4 1st Principal Stress (ksi)	Loading 4 2nd Principal Stress (ksi)	Loading 4 1st Principal Angle (rad)
G-10-2-D-N-K G-10-2-D-N-L G-10-2-D-N-M	27.06	4.37	-17.40	24.17	3.75	-17.49
G-10-2-D-N-N G-10-2-D-N-O G-10-2-D-N-P	28.49	3.31	-30.80	25.42	2.84	-30.75
G-11-1-D-S-K G-11-1-D-S-L G-11-1-D-S-M	25.51	4.79	-0.29	25.71	4.88	-0.27
G-11-1-D-S-N G-11-1-D-S-O G-11-1-D-S-P	33.28	6.12	-22.27	33.28	6.17	-22.10

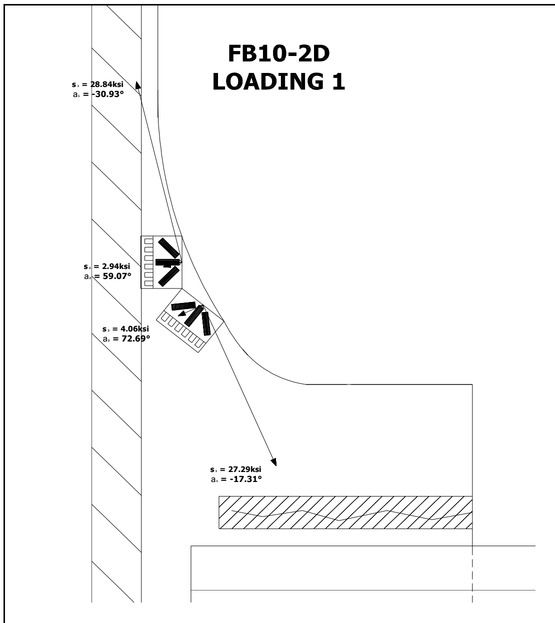

Figure 5.4.2: Principal Stress Magnitudes and Directions at Connections FB10-2-D-N

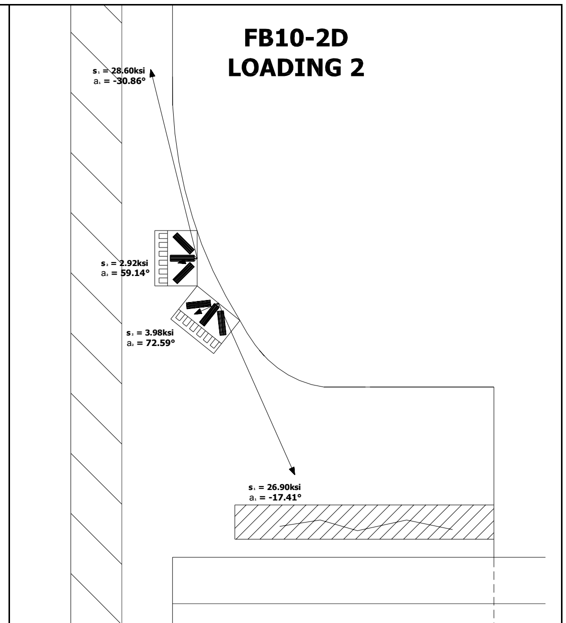

Figure 5.4.3: Principal Stress Magnitudes and Directions at Connections FB10-2-D-N

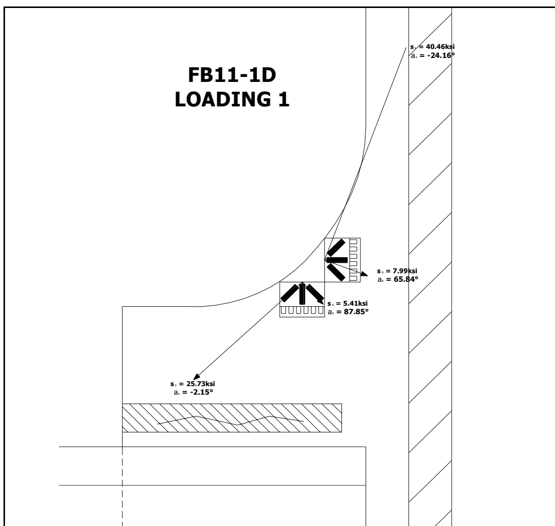

Figure 5.4.4: Principal Stress Magnitudes and Directions at Connections FB11-1-D-S

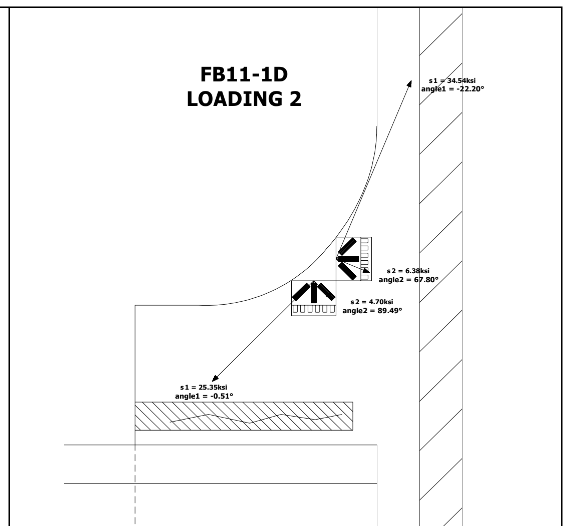

Figure 5.4.5: Principal Stress Magnitudes and Directions at Connections FB11-1-D-S

In these figures, the 1st principal stresses are tensile and tangent to the nearest surface, as would be expected. In addition, for each connection, the principal stresses and angles are similar in magnitude and direction, except for the upper rosette at FB11-1-D, loading condition 2, probably due to some non-linear near-yield strain at this location. Gage P in the rosette (see Figure 3.2.1) is the gage oriented closest to the 1st principal stress direction, which can be confirmed by evaluating the stress vs. time plot of each gage in the rosette. The plots are presented in Appendix A, with the largest stresses at gage P. Figure 5.4.6 is a time history plot of gage P for loadings 1 to 4 at connection FB11-1-D. Each peak in this plot corresponds to each of the four loadings of interest in this report. The small shift at 20 seconds occurred because one of the trucks drove back north to take position before another test was taken. Therefore a small amount of permanent strain developed between the first and second loading condition.

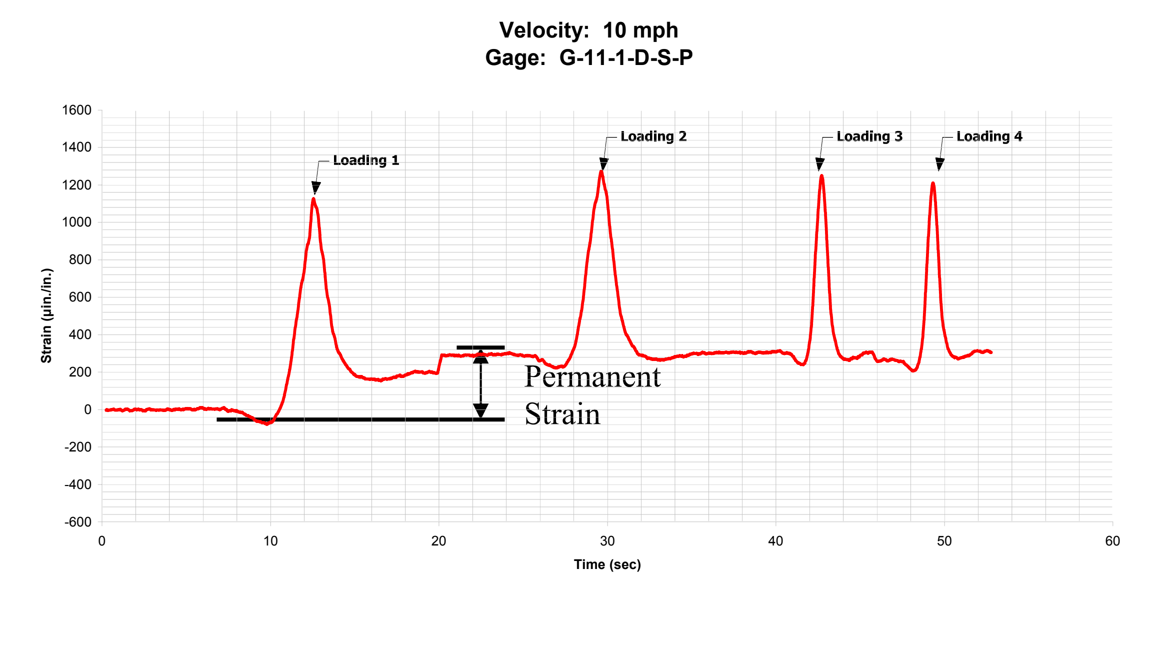

Figure 5.4.6: Strain History

The mill certification for the steel indicates an average yield stress of about 42 ksi. Table 5.4.1 shows a loading 1 maximum 1st principal stress for G-11-1-D of 40.5 ksi, so some yielding would be expected. As shown in Figure 5.4.6, permanent strain developed after the first loading. This permanent strain was included in the principal stress calculations. It is not reasonable to include this permanent strain in the fatigue life calculations because the fatigue life is dependent only on the stress range. For this reason, the principal stresses shown in Figure 5.4.4 for loading 1, FB11-1-D will not be used in the fatigue life calculations.

Fifteen loading were performed after retrofit, as listed in Appendix C. Figure 5.4.7 shows a strain versus time history graph of all loading conditions with each peak in the graph corresponding to each loading condition. This figure provides the unconditioned raw data that was recorded. The time of approximately 2.2 minutes on Figure 5.4.7, the graph shifts up to a permanent strain of about 1900 μin./in., which is the load case when two trucks are driving at 10 mph side by side.

The loading conditions 13 and 14, as indicated in Appendix C, occur when a 2”x10” board is placed across the driving lane above each of the test connections and a truck traveled over them at 5 mph. Loading condition 15 is when a 2”x10” board is placed across both lanes above FB11-1 test locations and two trucks traveled over them, side by side, at 5 mph. As observed in the Figure 5.4.7, the last loading exerted a great amount of permanent strain at one of the connections. These permanent strains, although unintended and undesirable, do indicate the successful softening of the floor-beam exterior connection, with a graceful permanent strain response to overload.

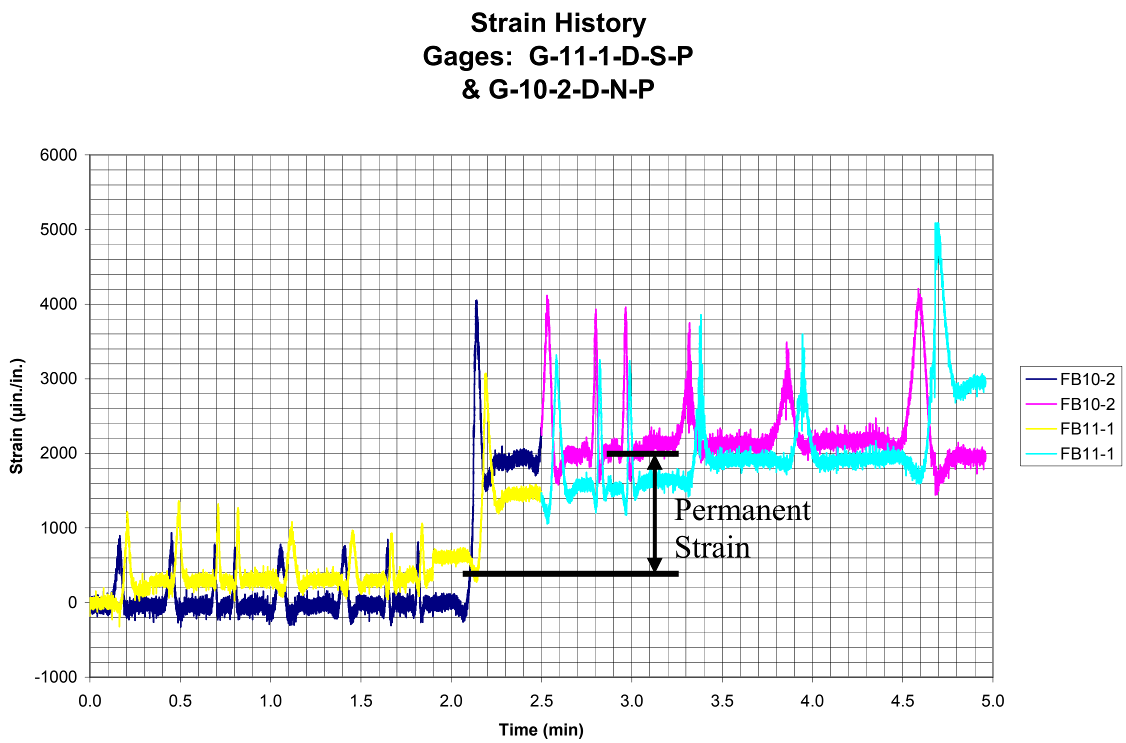

Figure 5.4.7: Gage P Strain History

5.5 Far-field Stress Ranges

Fatigue concepts and calculations for all AASHTO category details assume that the stress ranges are in the far-field regions where there are no effects due to stress concentrations as expressed in the following statement.

"These stresses are determined in fatigue tests on specimens simulating each detail in the group. Stress concentrations, residual stresses, initial flaws, and material variability are directly included in the tests." (Xanthakos, 1994)

Therefore, it is too conservative to use the measured principal stresses in the fatigue computations and scaling has been used to adjust the gage-measured stresses using the ANSYS model results. The scaling is done twice, using different assumptions, in an attempt to realistically bracket the future fatigue life behavior. The first assumption for scaling is that the

ANSYS model principal stress distribution and the actual stress contours are the same in properties but not in magnitude. The second assumption is that the measured stresses are directly related to the computed edge principal stresses.

For scaling based on the first assumption, the approximate location of the upper rosette gage, for each connection tested, is plotted on the ANSYS submodel as shown in Figure 5.5.1. Then the ANSYS model stresses at each rosette location are approximated and the edge ANSYS model stresses nearest to the location of each rosette are determined. Note that the 2” crack included in Figure 5.5.1 was shown in other ANSYS runs not to affect the stress field in the region used for scaling. The figure with the crack was included because it was available for reproduction purposes.

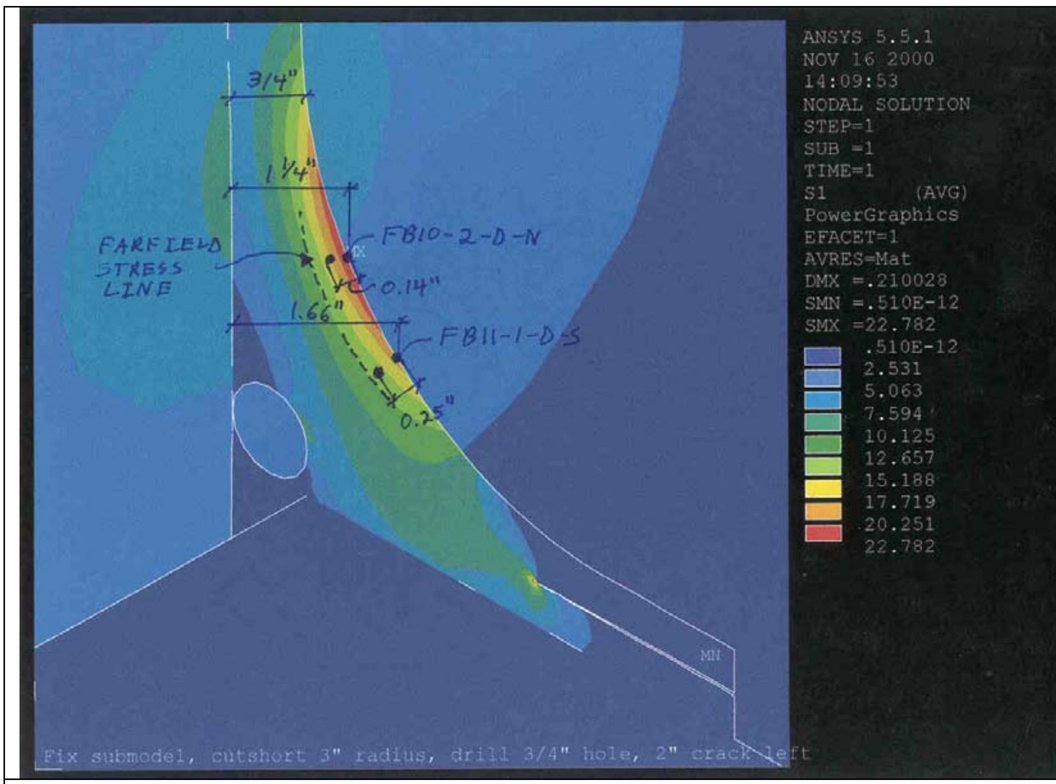

Figure 5.5.1: ANSYS Principal Stress Distribution After Retrofit (Zhao and Roddis, 2001, 2003)

For scaling, an adjusted edge stress is determined, which is dependent on the location of the gages, as expressed in Equation 5.5.1.

$$\sigma_{EADJ} = \frac{(\sigma_{EANSYS})*(\sigma_{M})}{(\sigma_{ANSYS})} \qquad \text{(Equation 5.5.1)}$$

To determine the far-field stress ranges, the measured stress ranges are used to scale the stress field computed using the ANSYS model.

$$\sigma_{FAR} = \frac{(\sigma_{EADJ})*(\sigma_{FARANSYS})}{(\sigma_{EANSYS})} \qquad \text{(Equation 5.5.2)}$$

Where:

σ_{M} = Measured Principal Stress

σ_{ANSYS} = Approximate Principal Stress at Location of Rosette in ANSYS Model

σ_{EANSYS} = Edge Principal Stress Nearest to Location of Rosette

σ_{EADJ}= Scaled Edge Principal Stress

$\sigma_{FARANSYS}$ = Far-field ANSYS Principal Stress

σ_{FAR}= Scaled Far-field Principal Stress

To determine the value to use for far-field stress from the ANSYS model, a conservative judgment was made to use 12 ksi, the value of the stress at the top of the curved transition cut on the plate, instead of the very low stresses at a distance of 10 times the plate thickness from the stress concentration. The results for this technique are provided in Table 5.5.1.

Table 5.5.1: First Far-field Stress Calculations

Connection	FB11-1-D-S	FB10-2-D-N
Perpendicular Distance from Edge of Stiffener (in.)	0.25	0.14
Width of Stiffener at Upper Rosette Location (in.)	1.66	1.25
σ_M (ksi)	34.54	28.84
σ_{ANSYS} (ksi)	13.90	17.70
σ_{EANSYS} (ksi)	18.60	22.70
σ_{EADJ} (ksi)	46.22	36.99
$\sigma_{FARANSYS}$ (ksi)	12.00	12.00
σ_{FAR} (ksi)	29.80	19.55

For the second scaling, it is assumed that the measured stresses are directly related to the edge principal stresses, as expressed in the following equation:

$$\sigma_{FAR} = \frac{(\sigma_M)*(\sigma_{FARANSYS})}{(\sigma_{EANSYS})} \qquad \text{(Equation 5.5.3)}$$

The results from scaling are provided in Table 5.5.2.

Table 5.5.2: Second Far-field Stress Calculations

Connection	FB11-1-D-S	FB10-2-D-N
Perpendicular Distance from Edge of Stiffener (in.)	0.25	0.14
Width of Stiffener at Upper Rosette Location (in.)	1.66	1.25
σ_M (ksi)	34.54	28.84
σ_{EANSYS} (ksi)	18.6	22.7
$\sigma_{FARANSYS}$ (ksi)	12.00	12.00
σ_{FAR} (ksi)	22.28	15.25

SECTION 6 FATIGUE LIFE COMPUTATIONS

The fatigue life calculations use the field measured strains and updated predicted traffic forecast information. The fatigue life calculated is for threshold life to crack initiation. Including crack propagation would not significantly change the fatigue life since the width of the partially cut plate near the exterior girder web is only ¾”.

The following equation is used to find the average daily truck traffic for a single lane (Zhao and Roddis, 2001, 2003):

$$(ADTT)_{SL} = \frac{(\%\text{Medium to Heavy Trucks}) * (\text{Daily Traffic})}{(\#\text{ of Lanes})} = \frac{(11\%)(12{,}500)}{(4)} = 344$$

(Equation 6.1)

The fatigue life prediction includes the existing Hutchinson bypass and the numbers are taken from a 2003 traffic survey conducted by KDOT. Table 6.1 provides the calculations using Equation 6.1 for the years of 2003, 2013, and 2023. This data for both the 2000 and 2003 KDOT traffic surveys are presented in Appendix B.

Table 6.1

Year	Predicted Daily Traffic	% Medium to Heavy Trucks	Average Daily Truck Traffic
2003	12,000	5	150
2013	14,000	5	175
2023	16,000	4.5	180

The year of 2023 was chosen for the fatigue threshold calculations because that year represents the worst scenario. The average daily truck traffic was reduced by 52% from 344 to 180.

The next calculation is the fatigue threshold life calculation scaled to the measured internal stresses. The equation to be used is given below:

$$N_Y = \frac{A}{\left[(365)(\Delta\sigma)^3 (ADTT)_{SL}\right]} \quad \text{(Equation 6.2)}$$

Where:

N_Y = Fatigue life

A = Constant = 250x10^8 for a category A detail in AASHTO Table 6.6.1.2.5-1

$\Delta\sigma$ = Stress range

$(ADTT)_{SL}$ = Average daily truck traffic

(AASHTO, 2000)

As discussed in Section 5.5, the far-field stress ranges were determined and the resultant fatigue life in provided in Table 6.2.

Table 6.2: Fatigue Life Results

Scaling Technique	Connection	Far-field Stress (ksi)	Fatigue Threshold Life (years)
1	FB11-1-D-N	29.8	29.7
1	FB10-2-D-N	19.6	24.6
2	FB11-1-D-N	22.3	62.4
2	FB10-2-D-N	15.3	59.1

These fatigue life calculations demonstrate the variability in calculated fatigue life, in this case due to the variability in the stress ranges. Fatigue life is a prediction based on the uncertain underlying assumptions in predicted traffic flow, recorded stresses, and approximations made in the AASHTO constants.

SECTION 7 CONCLUSIONS AND RECOMMENDATIONS

The field instrumentation analysis of the Arkansas River Bridge has been completed successfully. Equipment, testing set up, and testing procedures have been described. Gage and connection designations were clarified along with locations of strain gages before and after retrofit. Measured results due to an HS15 equivalent truck loading were compared to the analytical ANSYS model results. A fatigue life ranging between 25 years and 65 years was calculated based on measured strains and 2003 traffic data. Some permanent strain was induced onto the connection; therefore careful inspection must be performed with an emphasis on connection FB11-1 girder D.

The softening of the connections was successful. All other retrofit ideas presented in the previous computational report would have experienced greater stresses and shorter fatigue lives as indicated by the following:

> "This repair method shifts the location of the maximum stress range from a high concentration point Q4 to a mild curved surface point P4. The magnitude of the stress fluctuation is reduced and a better fatigue category is obtained after the cut-short. The crack opening stress at the original concentration point Q4 is now decreased to below the infinite life fatigue limit, so no crack should reinitiate from this point if the re-welding quality is good. However the other repair options have equal or worse construction difficulties. Compared to the other three repair plans, the retrofit method proposed in this section exhibits obvious advantages in reducing the stress variation, increasing the fatigue strength, controlling the crack reinitiation, and extending the useful service life. Therefore, this repair method is recommended for use in the actual bridge rehabilitation." (Zhao and Roddis, 2003)

SECTION 8 IMPLEMENTATION PLAN

The processes of analyzing data, elimination of the scatter, and judgments on the assumptions made in the calculations in the fatigue life can be used as a guide when similar tasks arise. Finite element computational analysis of cracking retrofits should always be done in conjunction with experimental stress analysis of the actual bridge connections. The importance of instrumentation analysis of bridges is particularly compelling when using a unique retrofit concept to enhance the lifetime of a bridge.

SECTION 9 REFERENCES

AASHTO Fatigue Guide, 1990

Guide Specifications for Fatigue Evaluation of Existing Steel Bridges, American Association of State Highway and Transportation Officials. Washington, D.C.

AASHTO LRFD Bridge Design Specifications, 2nd edition, 2000

American Association of State Highway and Transportation Officials. Washington, D.C.

Barson and Rolfe, 1999

Barson, John and Stanley Rolfe (1999). *Fracture and Fatigue Control in Structures: Applications of Fracture Mechanics*, 3rd Edition, ASTM, West Conshohocken, Pennsylvania.

Davis and Riley, 2001

Dally, James and William Riley (2001). *Experimental Stress Analysis*, 3rd *Edition*, College House Enterprises, LLC, Knoxville, Tennessee.

IOtech, Inc., 1997

IOtech, Inc. (1997). *Wave Book User's Manual*, Cleveland, Ohio.

Vishay Micro Measurements Group, Inc., 2000

Vishay Micro Measurements Group, Inc. (2000). *Product and Technical Binder*, Raleigh, North Carolina.

Xanthakos, 1994

Xanthakos, Petros. (1994). *Theory and Design of Bridges*, John Wiley & Sons, Inc., New York, New York.

Zhao and Roddis, 2001

Zhao, Yuan, and Kim Roddis. (2001). "*Investigation and Retrofit Recommendation for Cracking of the Arkansas River Bridge*," *SM Report* No. 60, The University of Kansas Center for Research, Inc., Lawrence, Kansas.

Zhao and Roddis, 2003

Zhao, Yuan, and Kim Roddis. (2003). *Fatigue-Prone Steel Bridge Details: Investigations and Recommended Repairs*, *Report No. K-TRAN: KU-99-2*, Kansas Department of Transportion, Topeka, Kansas.

APPENDIX A

Rosette gage plots for Loadings 1 and 2

This appendix provides a stress range versus time plot of each gage of the rosettes at both connections for loading conditions 1 and 2, to emphasize that gage P is in the direction and location closest to the highest principal stresses.

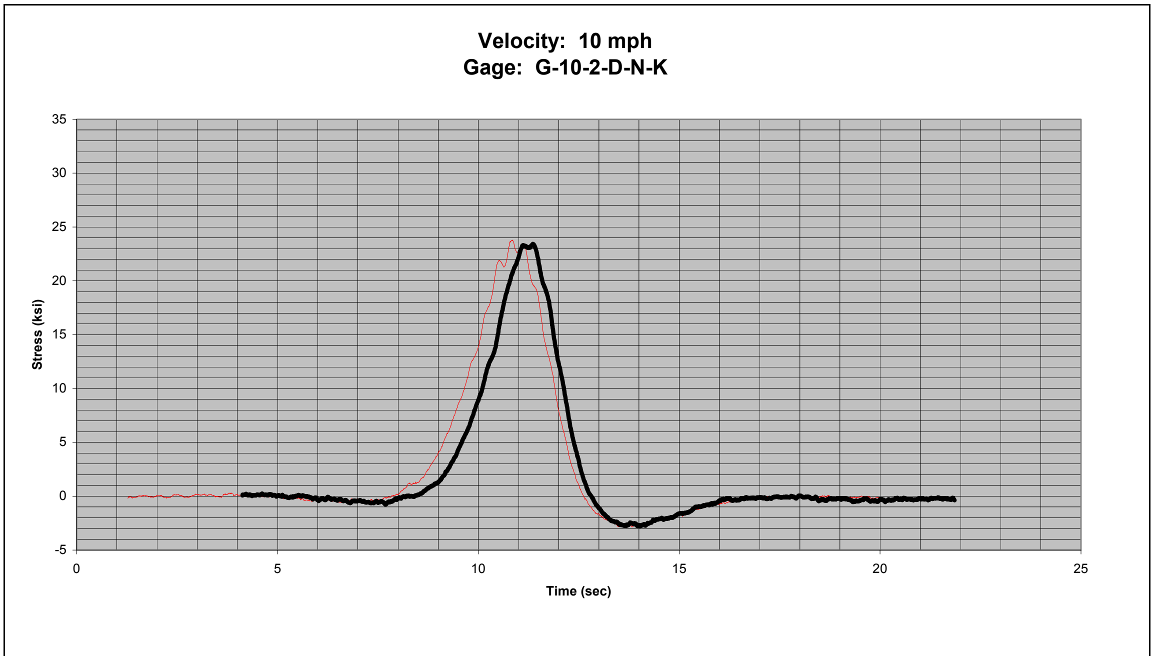
Velocity: 10 mph
Gage: G-10-2-D-N-K
35
30
25
20
15
10
5
0
-5
Stress (ksi)
0
5
10
15
20
25
Time (sec)

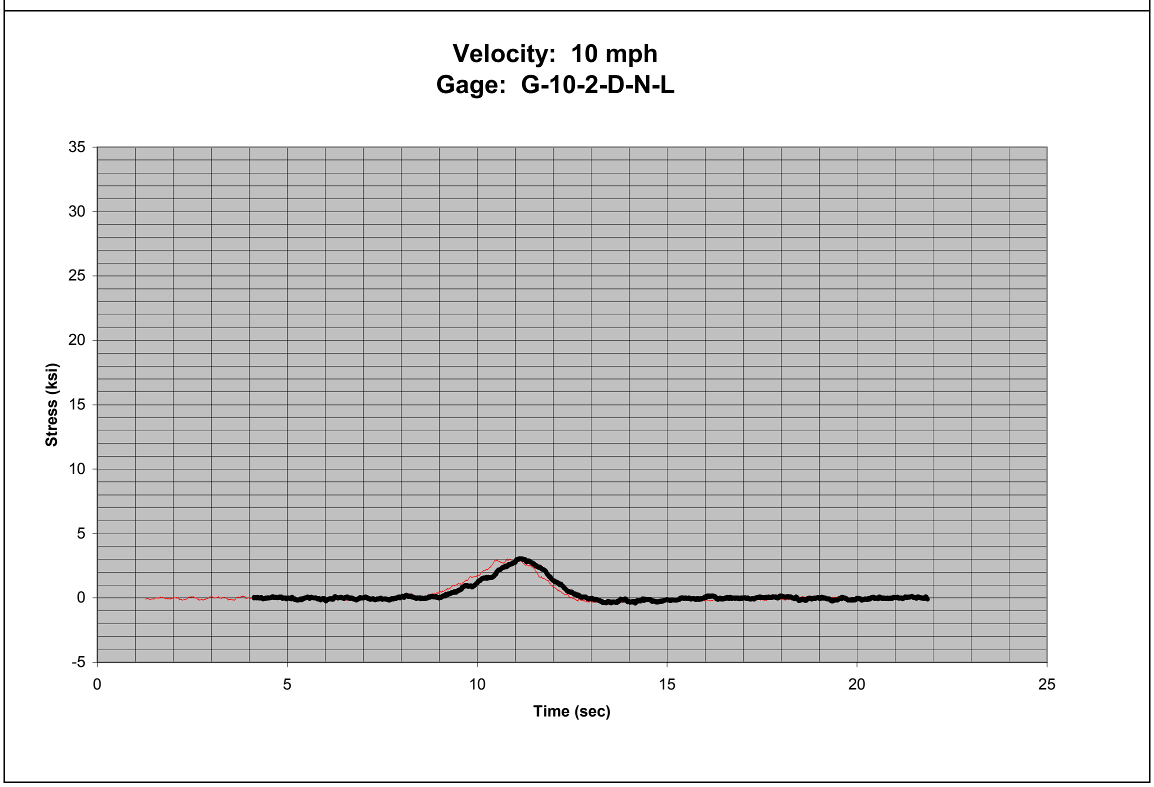
Velocity: 10 mph
Gage: G-10-2-D-N-L
35
30
25
20
15
10
5
0
-5
Stress (ksi)
0
5
10
15
20
25
Time (sec)

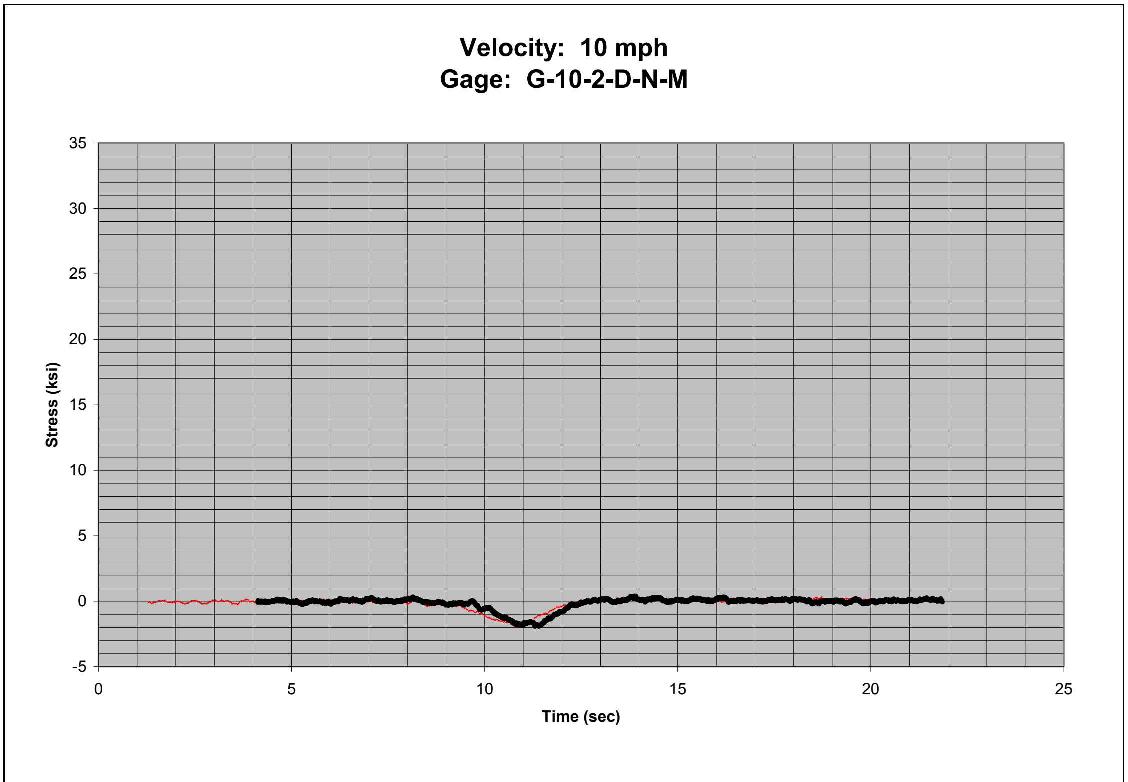
Velocity: 10 mph
Gage: G-10-2-D-N-M
Stress (ksi)
35
30
25
20
15
10
5
0
-5
0
5
10
15
20
25
Time (sec)

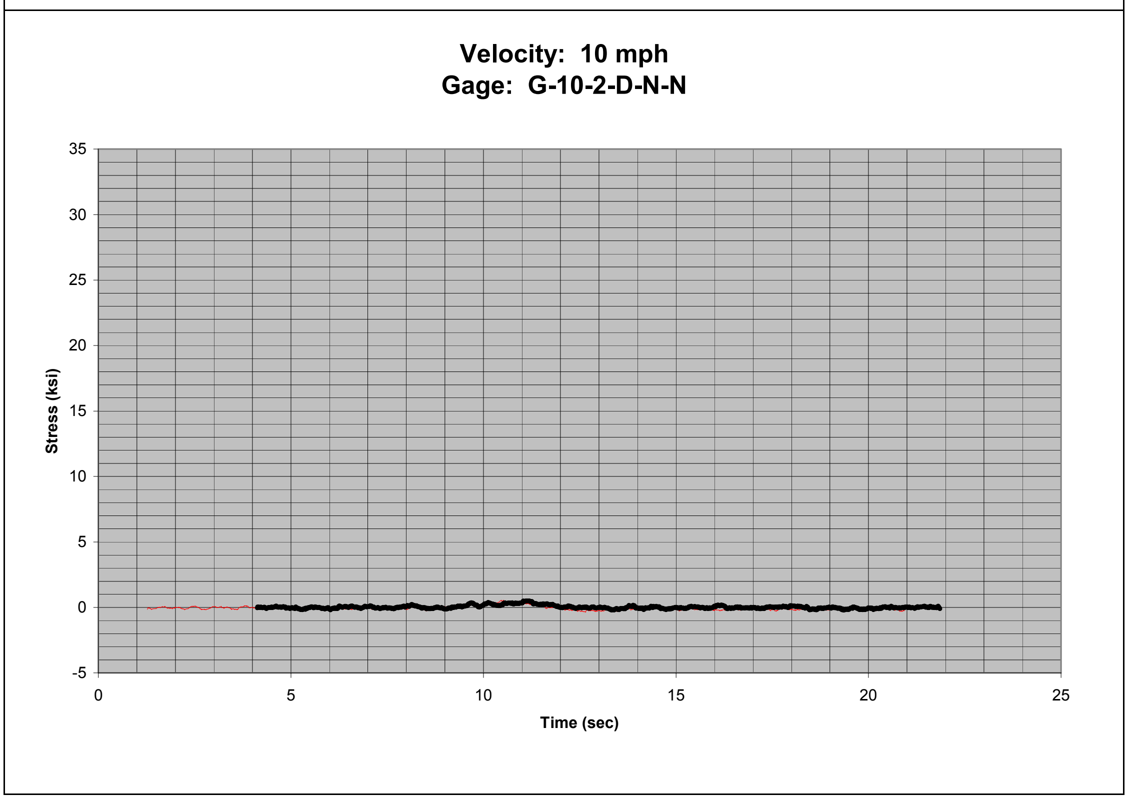
Velocity: 10 mph
Gage: G-10-2-D-N-N
Stress (ksi)
35
30
25
20
15
10
5
0
-5
0
5
10
15
20
25
Time (sec)

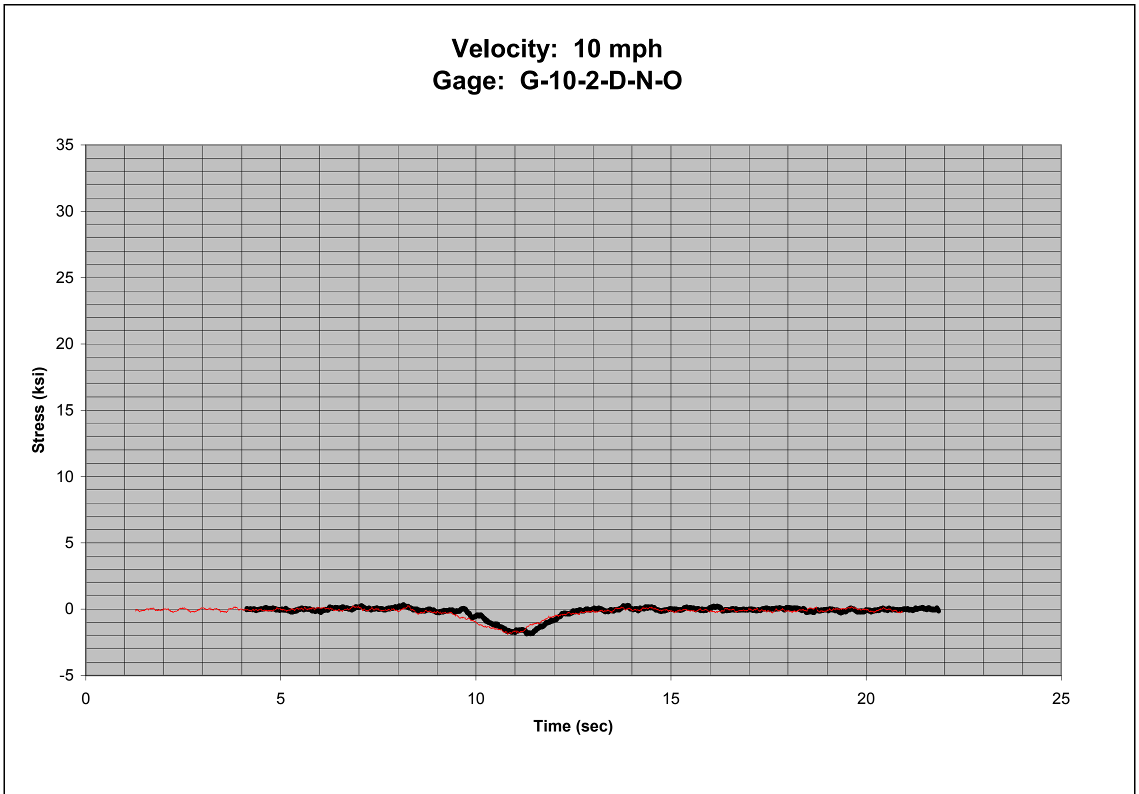
Velocity: 10 mph
Gage: G-10-2-D-N-O
35
30
25
20
15
10
5
0
-5
Stress (ksi)
0
5
10
15
20
25
Time (sec)

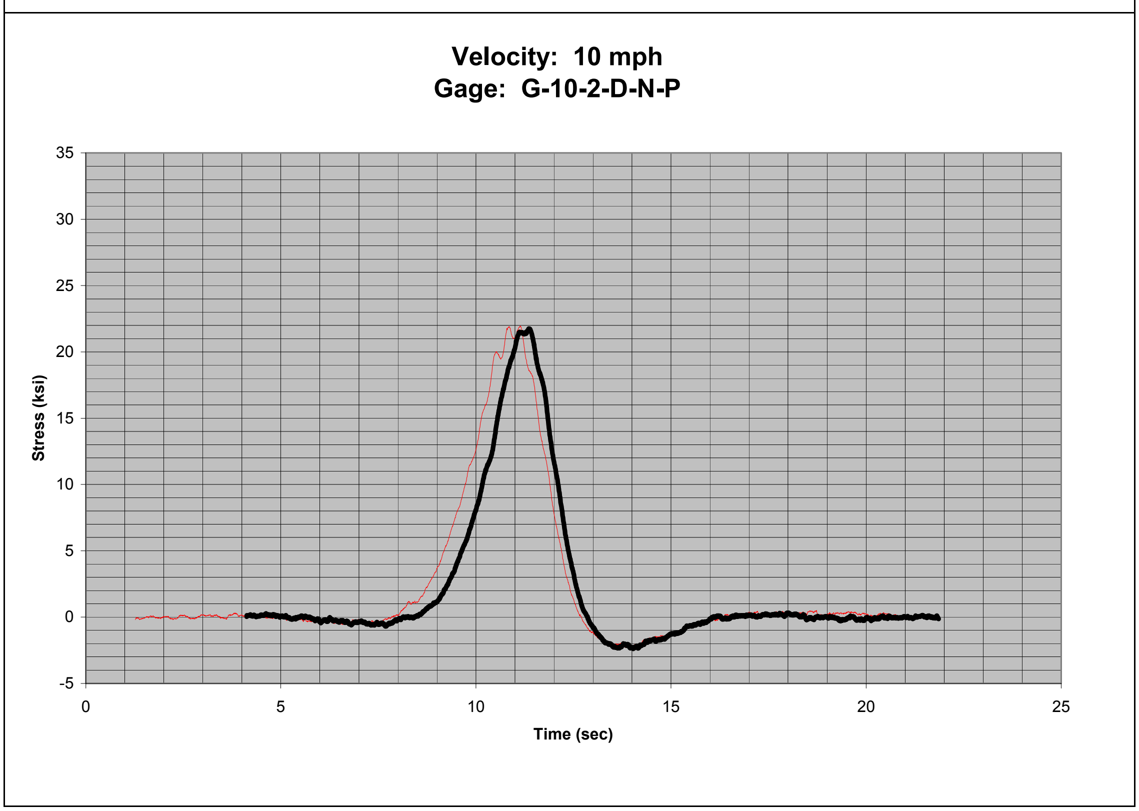
Velocity: 10 mph
Gage: G-10-2-D-N-P
35
30
25
20
15
10
5
0
-5
Stress (ksi)
0
5
10
15
20
25
Time (sec)

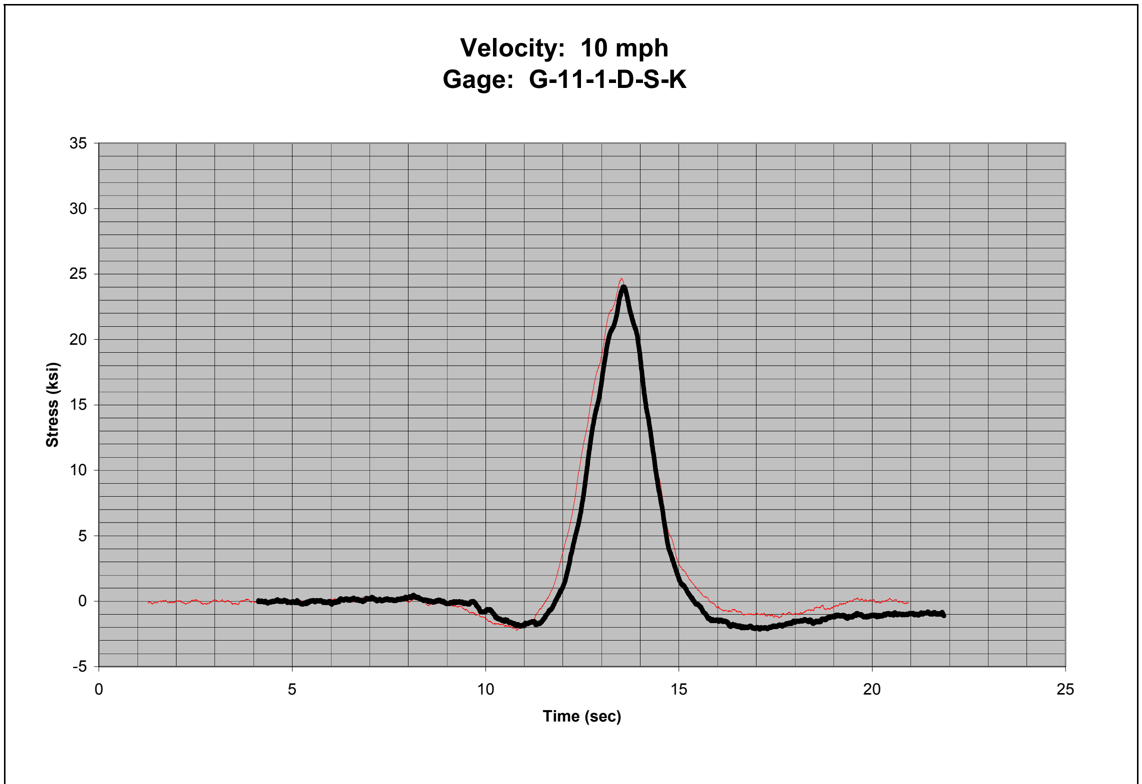
Velocity: 10 mph
Gage: G-11-1-D-S-K
Stress (ksi)
Time (sec)

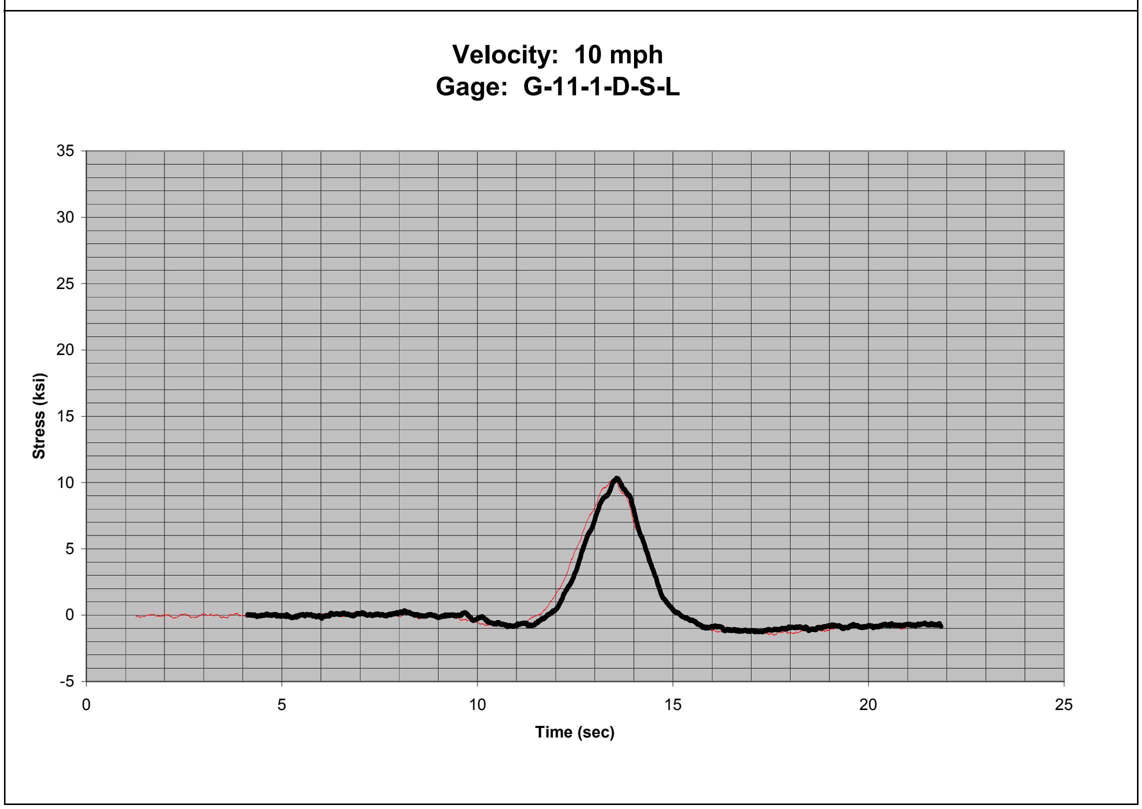
Velocity: 10 mph
Gage: G-11-1-D-S-L
Stress (ksi)
Time (sec)

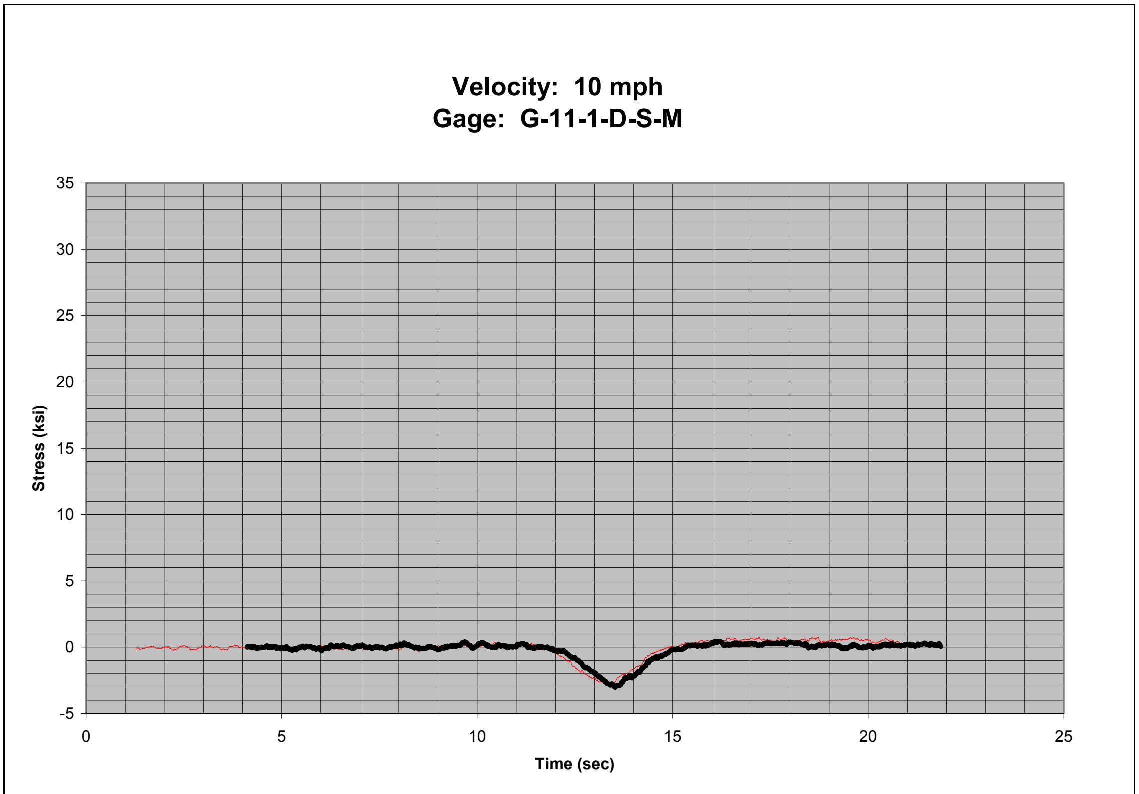

Velocity: 10 mph
Gage: G-11-1-D-S-M
Stress (ksi)
Time (sec)

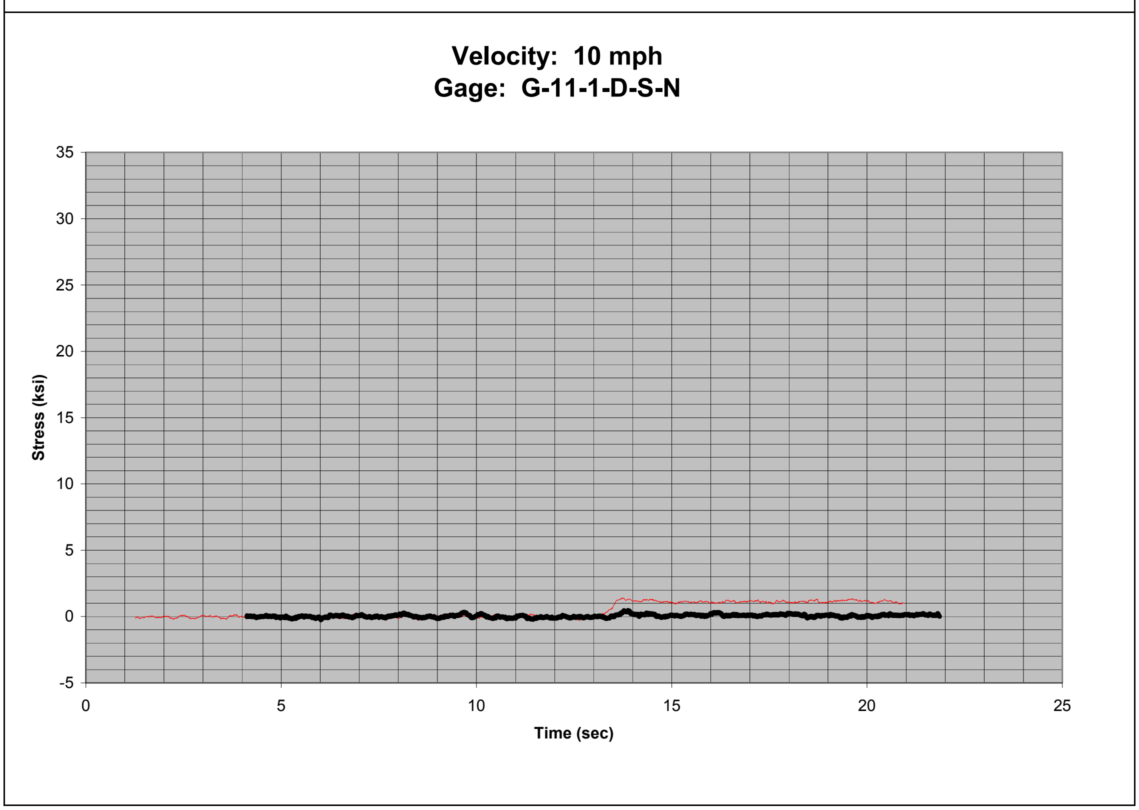

Velocity: 10 mph
Gage: G-11-1-D-S-N
Stress (ksi)
Time (sec)

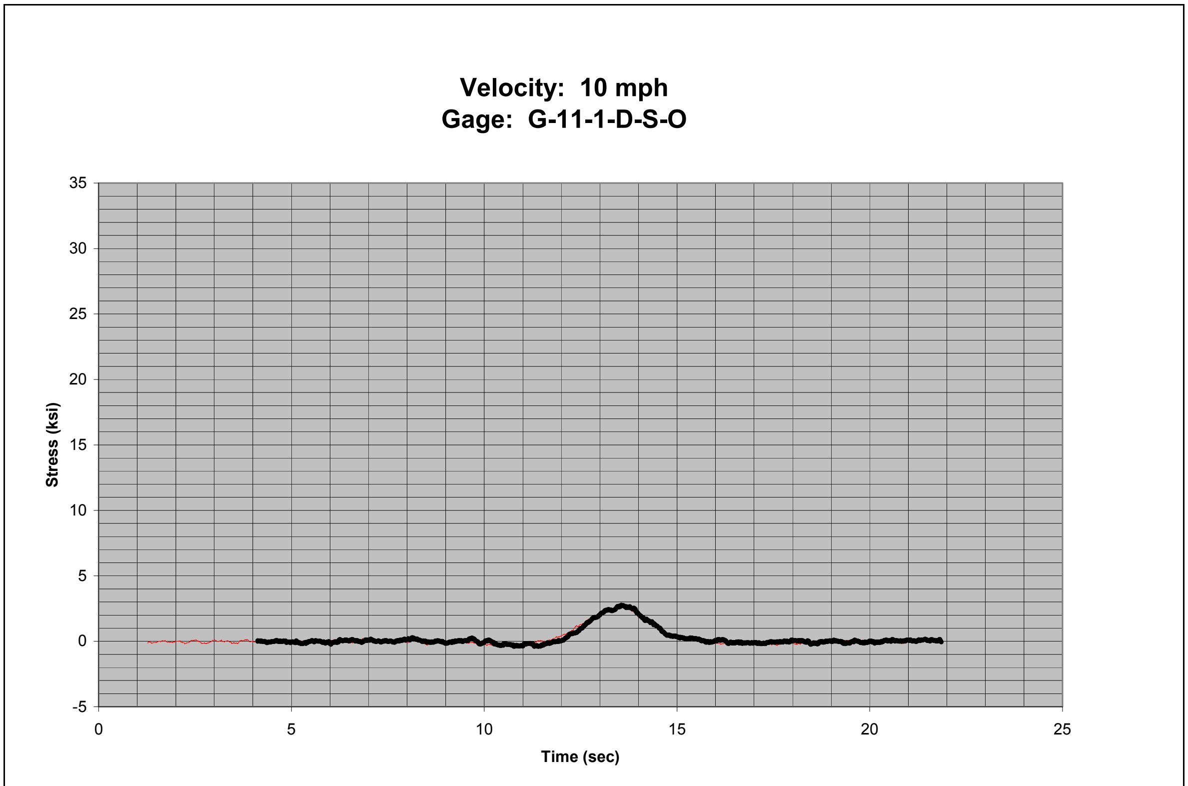
Velocity: 10 mph
Gage: G-11-1-D-S-O
Stress (ksi)
Time (sec)
35
30
25
20
15
10
5
0
-5
0
5
10
15
20
25

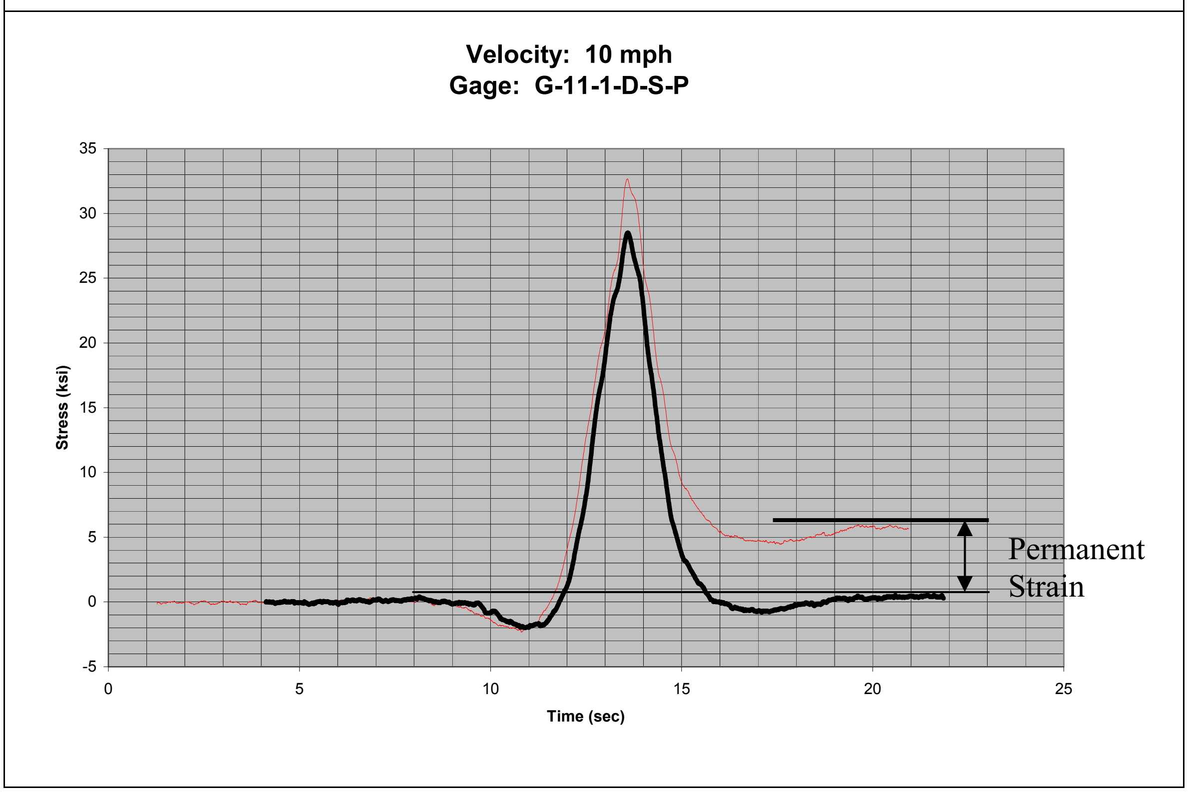
Velocity: 10 mph
Gage: G-11-1-D-S-P
Stress (ksi)
Time (sec)
Permanent
Strain
35
30
25
20
15
10
5
0
-5
0
5
10
15
20
25

APPENDIX B

Traffic Forecast for the Years 2003-2023

The following appendix provides traffic forecasts assuming the Hutchinson bypass exists and does not exists. The first one as performed by KDOT in 2000 and the second one was performed by KDOT in 2003.

EQUIVALENT SINGLE AXLE LOADS (ESAL) ANALYSIS

South Hutchinson K-96 Bridge over the Arkansas River

96-78 K-6879-01 Assuming Hutchinson Bypass

		% DIST.	18 KIP ADL ON RIGID PVMNT.*		18 KIP ADL ON FLEX. PVMNT.*	
YR 2003 TRAFFIC =	12000	10.0% TRUCKS	D=260mm (10in.)	D=280mm (11in.)	SN=5	SN=6
AUTO	8064	67.2	2.42	2.42	2.42	2.42
LT. TRUCK	2736	22.8	5.47	5.47	5.47	5.47
2 AXLE-6 TIRE	204	1.7	37.74	38.15	36.11	36.31
3 AXLE TANDEM	48	0.4	38.02	38.78	24.14	26.20
4 AXLE 1 TRAILER	168	1.4	122.64	123.31	108.86	111.22
5 AXLE 1 TRAILER	684	5.7	1411.78	1424.77	844.74	861.16
5 AXLE 2 TRAILER	36	0.3	60.23	60.26	60.88	59.69
6 AXLE 2 TRAILER	60	0.5	111.12	111.24	91.74	93.00
TOTALS	12000	100.0	1789.41	1804.41	1174.36	1194.46

		% DIST.	18 KIP ADL ON RIGID PVMNT.*		18 KIP ADL ON FLEX. PVMNT.*	
YR 2013 TRAFFIC =	14000	10.0% TRUCKS	D=260mm (10in.)	D=280mm (11in.)	SN=5	SN=6
AUTO	9408	67.2	2.82	2.82	2.82	2.82
LT. TRUCK	3192	22.8	6.38	6.38	6.38	6.38
2 AXLE-6 TIRE	238	1.7	44.03	44.51	42.13	42.36
3 AXLE TANDEM	56	0.4	44.35	45.25	28.17	29.40
4 AXLE 1 TRAILER	196	1.4	143.08	143.86	127.01	129.75
5 AXLE 1 TRAILER	798	5.7	1647.07	1662.23	985.53	1004.68
5 AXLE 2 TRAILER	42	0.3	70.27	70.31	71.02	69.64
6 AXLE 2 TRAILER	70	0.5	129.64	129.78	107.03	108.50
TOTALS	14000	100.0	2087.65	2105.15	1370.09	1393.54

10 YEAR ACCUMULATED ESAL'S	
RIGID PAVEMENT:	
D=260mm:	7,075,630
D=280mm:	7,134,943
FLEXIBLE PAVEMENT:	
SN=5 :	4,643,628
SN=6 :	4,723,107

		% DIST.	18 KIP ADL ON RIGID PVMNT.*		18 KIP ADL ON FLEX. PVMNT.*	
YR 2023 TRAFFIC =	16000	9.0% TRUCKS	D=260mm (10in.)	D=280mm (11in.)	SN=5	SN=6
AUTO	10880	68.0	3.26	3.26	3.26	3.26
LT. TRUCK	3680	23.0	7.36	7.36	7.36	7.36
2 AXLE-6 TIRE	240	1.5	44.40	44.88	42.48	42.72
3 AXLE TANDEM	64	0.4	50.69	51.71	32.19	33.60
4 AXLE 1 TRAILER	208	1.3	151.84	152.67	134.78	137.70
5 AXLE 1 TRAILER	800	5.0	1651.20	1666.40	988.00	1007.20
5 AXLE 2 TRAILER	48	0.3	80.30	80.35	81.17	79.58
6 AXLE 2 TRAILER	80	0.5	148.16	148.32	122.32	124.00
TOTALS	16000	100.0	2137.22	2154.96	1411.57	1435.42

20 YEAR ACCUMULATED ESAL'S	
RIGID PAVEMENT:	
D=260mm:	14,332,189
D=280mm:	14,451,705
FLEXIBLE PAVEMENT:	
SN=5 :	9,438,649
SN=6 :	9,599,088

* USING TERMINAL SERVICEABILITY OF 2.5 / FACILITY TYPE RURAL
USING 1992, 1993, & 1994 KANSAS TRUCK WEIGHT DATA

27-SEP-00

O:\Forecasts\Hutchinson\K96BRBYP.WB2

EQUIVALENT SINGLE AXLE LOADS (ESAL) ANALYSIS
South Hutchinson K-96 Bridge over the Arkansas River
96-78 K-6879-01 Assuming NO Hutchinson Bypass

		% DIST.	18 KIP ADL ON RIGID PVMNT.*		18 KIP ADL ON FLEX. PVMNT.*	
YR 2003 TRAFFIC =	13600	11.0% TRUCKS	D=260mm (10in.)	D=280mm (11in.)	SN=5	SN=6
AUTO	9044	66.5	2.71	2.71	2.71	2.71
LT. TRUCK	3060	22.5	6.12	6.12	6.12	6.12
2 AXLE-6 TIRE	258	1.9	47.80	48.32	45.74	46.00
3 AXLE TANDEM	68	0.5	53.86	54.94	34.20	35.70
4 AXLE 1 TRAILER	204	1.5	148.92	149.74	132.19	135.05
5 AXLE 1 TRAILER	843	6.2	1740.36	1756.39	1041.35	1061.59
5 AXLE 2 TRAILER	41	0.3	68.26	68.30	68.99	67.65
6 AXLE 2 TRAILER	82	0.6	151.12	151.29	124.77	126.48
TOTALS	13600	100.0	2219.16	2237.81	1456.08	1481.29

		% DIST.	18 KIP ADL ON RIGID PVMNT.*		18 KIP ADL ON FLEX. PVMNT.*	
YR 2013 TRAFFIC =	15900	11.0% TRUCKS	D=260mm (10in.)	D=280mm (11in.)	SN=5	SN=6
AUTO	10574	66.5	3.17	3.17	3.17	3.17
LT. TRUCK	3578	22.5	7.16	7.16	7.16	7.16
2 AXLE-6 TIRE	302	1.9	55.89	56.49	53.47	53.77
3 AXLE TANDEM	80	0.5	62.96	64.24	39.99	41.74
4 AXLE 1 TRAILER	239	1.5	174.11	175.06	154.55	157.89
5 AXLE 1 TRAILER	986	6.2	2034.69	2053.42	1217.46	1241.12
5 AXLE 2 TRAILER	48	0.3	79.80	79.85	80.66	79.09
6 AXLE 2 TRAILER	95	0.6	176.68	176.87	145.87	147.87
TOTALS	15900	100.0	2594.46	2616.26	1702.33	1731.80

10 YEAR ACCUMULATED ESAL'S	
RIGID PAVEMENT:	
D=260mm:	8,784,853
D=280mm:	8,858,665
FLEXIBLE PAVEMENT:	
SN=5 :	5,764,085
SN=6 :	5,863,900

		% DIST.	18 KIP ADL ON RIGID PVMNT.*		18 KIP ADL ON FLEX. PVMNT.*	
YR 2023 TRAFFIC =	18300	11.0% TRUCKS	D=260mm (10in.)	D=280mm (11in.)	SN=5	SN=6
AUTO	12170	66.5	3.65	3.65	3.65	3.65
LT. TRUCK	4118	22.5	8.24	8.24	8.24	8.24
2 AXLE-6 TIRE	348	1.9	64.32	65.02	61.54	61.89
3 AXLE TANDEM	92	0.5	72.47	73.93	46.02	48.04
4 AXLE 1 TRAILER	275	1.5	200.39	201.48	177.88	181.72
5 AXLE 1 TRAILER	1135	6.2	2341.81	2363.37	1401.23	1428.46
5 AXLE 2 TRAILER	55	0.3	91.85	91.90	92.84	91.02
6 AXLE 2 TRAILER	110	0.6	203.35	203.57	167.88	170.19
TOTALS	18300	100.0	2986.08	3011.16	1959.28	1993.21

20 YEAR ACCUMULATED ESAL'S	
RIGID PAVEMENT:	
D=260mm:	18,999,106
D=280mm:	19,158,739
FLEXIBLE PAVEMENT:	
SN=5 :	12,466,055
SN=6 :	12,681,926

* USING TERMINAL SERVICEABILITY OF 2.5 / FACILITY TYPE RURAL
USING 1992, 1993, & 1994 KANSAS TRUCK WEIGHT DATA

27-SEP-00

O:\Forecasts\Hutchinson\K96BR.WB2

EQUIVALENT SINGLE AXLE LOADS (ESAL) ANALYSIS

South Hutchinson K-96 Bridge over the Arkansas River

96-78 K-6879-01 Assuming Hutchinson Bypass

		% DIST.	18 KIP ADL ON RIGID PVMNT.*		18 KIP ADL ON FLEX. PVMNT.*	
YR 2003 TRAFFIC =	12000	5.0% TRUCKS	D=260mm (10in.)	D=280mm (11in.)	SN=5	SN=6
AUTO	8520	71.0	2.56	2.56	2.56	2.56
LT. TRUCK	2880	24.0	5.76	5.76	5.76	5.76
2 AXLE-6 TIRE	108	0.9	24.52	24.62	24.08	23.98
3 AXLE TANDEM	24	0.2	28.63	29.09	17.98	18.53
4 AXLE 1 TRAILER	84	0.7	61.24	61.32	56.70	57.20
5 AXLE 1 TRAILER	336	2.8	727.10	734.50	430.42	441.17
5 AXLE 2 TRAILER	12	0.1	26.28	26.32	26.14	26.05
6 AXLE 2 TRAILER	36	0.3	106.45	106.96	84.42	84.60
TOTALS	12000	100.0	982.54	991.12	648.05	659.84

		% DIST.	18 KIP ADL ON RIGID PVMNT.*		18 KIP ADL ON FLEX. PVMNT.*	
YR 2013 TRAFFIC =	14000	5.0% TRUCKS	D=260mm (10in.)	D=280mm (11in.)	SN=5	SN=6
AUTO	9940	71.0	2.98	2.98	2.98	2.98
LT. TRUCK	3360	24.0	6.72	6.72	6.72	6.72
2 AXLE-6 TIRE	126	0.9	28.60	28.73	28.10	27.97
3 AXLE TANDEM	28	0.2	33.40	33.94	20.97	21.62
4 AXLE 1 TRAILER	98	0.7	71.44	71.54	66.15	66.74
5 AXLE 1 TRAILER	392	2.8	848.29	856.91	502.15	514.70
5 AXLE 2 TRAILER	14	0.1	30.66	30.70	30.49	30.39
6 AXLE 2 TRAILER	42	0.3	124.19	124.78	98.49	98.70
TOTALS	14000	100.0	1146.29	1156.30	756.06	769.82

10 YEAR ACCUMULATED ESAL'S	
RIGID PAVEMENT:	
D=260mm:	3,885,111
D=280mm:	3,919,038
FLEXIBLE PAVEMENT:	
SN=5 :	2,562,490
SN=6 :	2,609,133

		% DIST.	18 KIP ADL ON RIGID PVMNT.*		18 KIP ADL ON FLEX. PVMNT.*	
YR 2023 TRAFFIC =	16000	4.5% TRUCKS	D=260mm (10in.)	D=280mm (11in.)	SN=5	SN=6
AUTO	11408	71.3	3.42	3.42	3.42	3.42
LT. TRUCK	3872	24.2	7.74	7.74	7.74	7.74
2 AXLE-6 TIRE	128	0.8	29.06	29.18	28.54	28.42
3 AXLE TANDEM	32	0.2	38.18	38.78	23.97	24.70
4 AXLE 1 TRAILER	96	0.6	69.98	70.08	64.80	65.38
5 AXLE 1 TRAILER	416	2.6	900.22	909.38	532.90	546.21
5 AXLE 2 TRAILER	16	0.1	35.04	35.09	34.85	34.74
6 AXLE 2 TRAILER	32	0.2	94.62	95.07	75.04	75.20
TOTALS	16000	100.0	1178.27	1188.75	771.26	785.81

20 YEAR ACCUMULATED ESAL'S	
RIGID PAVEMENT:	
D=260mm:	7,886,943
D=280mm:	7,956,512
FLEXIBLE PAVEMENT:	
SN=5 :	5,180,483
SN=6 :	5,276,624

* USING TERMINAL SERVICEABILITY OF 2.5 / FACILITY TYPE URBAN
USING 1992, 1993, & 1994 KANSAS TRUCK WEIGHT DATA

28-Apr-03

O:\Forecasts\Hutchinson\K96BRBYP.WB2

EQUIVALENT SINGLE AXLE LOADS (ESAL) ANALYSIS

South Hutchinson K-96 Bridge over the Arkansas River

96-78 K-6879-01 Assuming NO Hutchinson Bypass

		% DIST.	18 KIP ADL ON RIGID PVMNT.*		18 KIP ADL ON FLEX. PVMNT.*	
YR 2003 TRAFFIC =	13600	6.5% TRUCKS	D=260mm (10in.)	D=280mm (11in.)	SN=5	SN=6
AUTO	9493	69.8	2.85	2.85	2.85	2.85
LT. TRUCK	3223	23.7	6.45	6.45	6.45	6.45
2 AXLE-6 TIRE	150	1.1	33.96	34.11	33.36	33.21
3 AXLE TANDEM	41	0.3	48.67	49.45	30.56	31.50
4 AXLE 1 TRAILER	122	0.9	89.23	89.35	82.62	83.35
5 AXLE 1 TRAILER	503	3.7	1088.92	1100.00	644.60	660.70
5 AXLE 2 TRAILER	27	0.2	59.57	59.65	59.24	59.05
6 AXLE 2 TRAILER	41	0.3	120.65	121.22	95.68	95.88
TOTALS	13600	100.0	1450.30	1463.07	955.35	972.99

		% DIST.	18 KIP ADL ON RIGID PVMNT.*		18 KIP ADL ON FLEX. PVMNT.*	
YR 2013 TRAFFIC =	15900	6.5% TRUCKS	D=260mm (10in.)	D=280mm (11in.)	SN=5	SN=6
AUTO	11098	69.8	3.33	3.33	3.33	3.33
LT. TRUCK	3768	23.7	7.54	7.54	7.54	7.54
2 AXLE-6 TIRE	175	1.1	39.70	39.88	39.00	38.83
3 AXLE TANDEM	48	0.3	56.91	57.81	35.73	36.82
4 AXLE 1 TRAILER	143	0.9	104.32	104.46	96.59	97.45
5 AXLE 1 TRAILER	588	3.7	1273.08	1286.02	753.61	772.44
5 AXLE 2 TRAILER	32	0.2	69.64	69.74	69.26	69.04
6 AXLE 2 TRAILER	48	0.3	141.05	141.72	111.86	112.09
TOTALS	15900	100.0	1695.57	1710.50	1116.92	1137.54

10 YEAR ACCUMULATED ESAL'S	
RIGID PAVEMENT:	
D=260mm:	5,741,199
D=280mm:	5,791,752
FLEXIBLE PAVEMENT:	
SN=5 :	3,781,891
SN=6 :	3,851,718

		% DIST.	18 KIP ADL ON RIGID PVMNT.*		18 KIP ADL ON FLEX. PVMNT.*	
YR 2023 TRAFFIC =	18300	6.5% TRUCKS	D=260mm (10in.)	D=280mm (11in.)	SN=5	SN=6
AUTO	12773	69.8	3.83	3.83	3.83	3.83
LT. TRUCK	4337	23.7	8.67	8.67	8.67	8.67
2 AXLE-6 TIRE	201	1.1	45.70	45.90	44.89	44.69
3 AXLE TANDEM	55	0.3	65.50	66.54	41.12	42.38
4 AXLE 1 TRAILER	165	0.9	120.07	120.23	111.17	112.16
5 AXLE 1 TRAILER	677	3.7	1465.24	1480.14	867.37	889.03
5 AXLE 2 TRAILER	37	0.2	80.15	80.26	79.71	79.46
6 AXLE 2 TRAILER	55	0.3	162.34	163.11	128.74	129.02
TOTALS	18300	100.0	1951.50	1968.68	1285.51	1309.24

20 YEAR ACCUMULATED ESAL'S	
RIGID PAVEMENT:	
D=260mm:	12,416,559
D=280mm:	12,525,891
FLEXIBLE PAVEMENT:	
SN=5 :	8,179,140
SN=6 :	8,330,156

* USING TERMINAL SERVICEABILITY OF 2.5 / FACILITY TYPE URBAN
USING 1992, 1993, & 1994 KANSAS TRUCK WEIGHT DATA

28-APR-03

O:\Forecasts\Hutchinson\K96BR.WB2

APPENDIX C

Loading Conditions After Retrofit

The following appendix provides all the loading conditions that were performed after retrofit.

Loading Condition	Truck Number	Velocity (mph)	Description of Loading Condition And Lanes Occupied	Duration of Recording (sec.)	Calculated Velocity (mph)
1	1	10	Driving Lane	35	11.76
2	2	10	Driving Lane	35	11.76
3	1	30	Driving Lane	15	27.44
4	2	30	Driving Lane	15	27.44
5	1	10	Passing Lane	36	11.43
6	2	10	Passing Lane	30	13.72
7	1	30	Passing Lane	14	29.40
8	2	30	Passing Lane	16	25.73
9	Both	10	Driving Side by Side	37	11.12
10	Both	10	Driving Side by Side	38	10.83
11	Both	25	Driving Side by Side	18	22.87
12	Both	25	Driving Side by Side	18	22.87
13	2	5	Running Over 2"x12" Lumber Placed Above FB10-2 and FB11-1 Test Locations in Driving Lane.	54	7.62
14	1	5	Running Over 2"x12" Lumber Placed Above FB10-2 and FB11-1 Test Locations in Driving Lane.	74	5.56
15	Both	5	Running Over 2"x12" Lumber Placed Above FB11-1 Test Locations in Both Lanes.	75	5.49
Loadings After Retrofit					

APPENDIX D

Arkansas River Bridge Repair Drawings

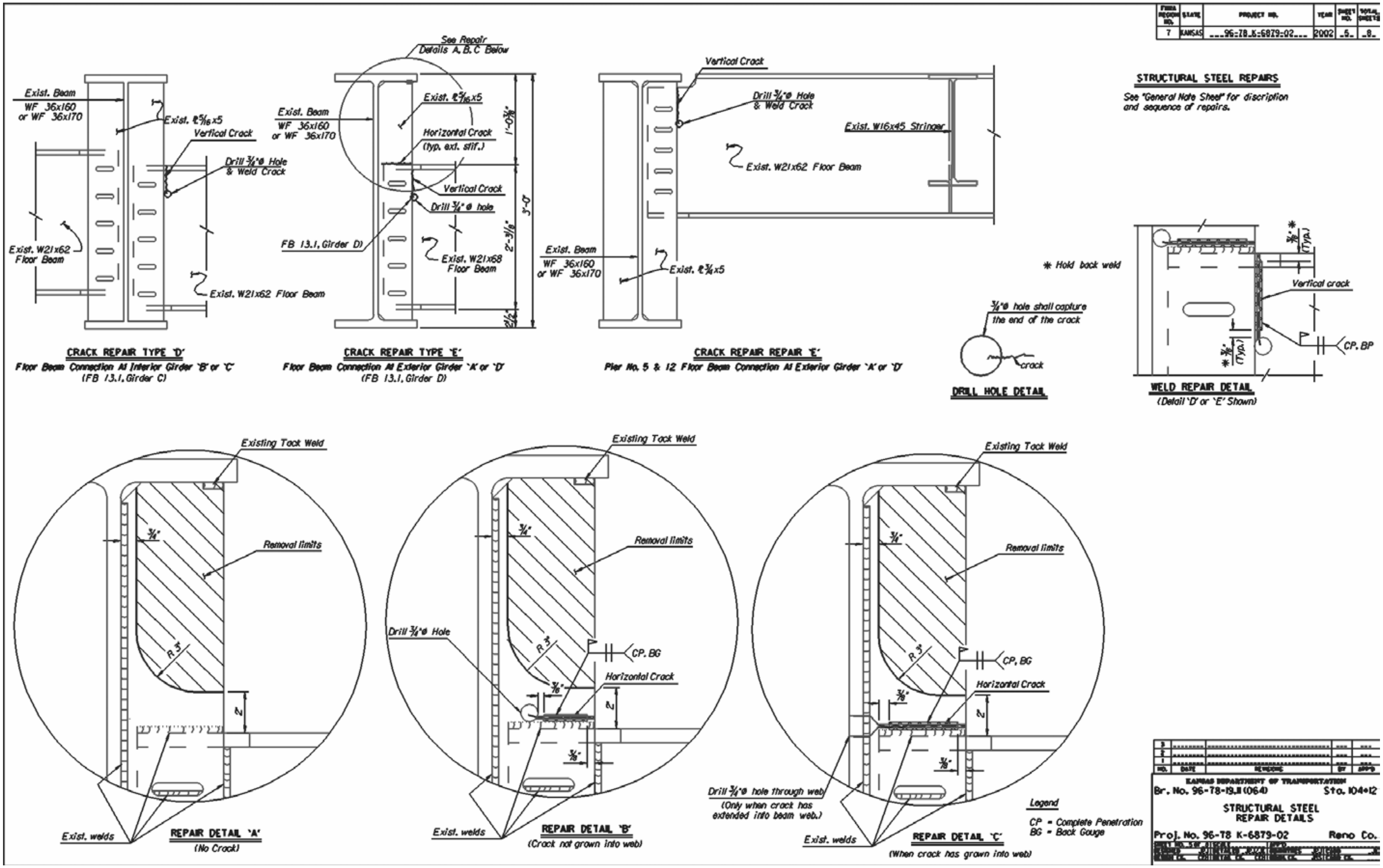
STRUCTURAL STEEL REPAIRS
See "General Note Sheet" for discription and sequence of repairs.
CRACK REPAIR TYPE 'D'
Floor Beam Connection At Interior Girder 'B' or 'C'
(FB 13.1, Girder C)
CRACK REPAIR TYPE 'E'
Floor Beam Connection At Exterior Girder 'A' or 'D'
(FB 13.1, Girder D)
CRACK REPAIR REPAIR 'E'
Pier No. 5 & 12 Floor Beam Connection At Exterior Girder 'A' or 'D'
DRILL HOLE DETAIL
WELD REPAIR DETAIL
(Detail 'D' or 'E' Shown)
REPAIR DETAIL 'A'
(No Crack)
REPAIR DETAIL 'B'
(Crack not grown into web)
REPAIR DETAIL 'C'
(When crack has grown into web)
Legend
CP = Complete Penetration
BG = Back Gouge
Br. No. 96-78-19.II (064)
Sta. 104+12
STRUCTURAL STEEL REPAIR DETAILS
Proj. No. 96-78 K-6879-02
Reno Co.